H3K9me2 orchestrates inheritance of spatial positioning of peripheral heterochromatin through mitosis

Andrey Poleshko[1], Cheryl L. Smith[1], Son C. Nguyen[2], Priya Sivaramakrishnan[2], John Isaac Murray[2], Melike Lakadamyali[3], Eric F. Joyce[2], Rajan Jain[1,4*], and Jonathan A. Epstein[1,4*]

[1]Department of Cell and Developmental Biology, Perelman School of Medicine, University of Pennsylvania, Philadelphia, Pennsylvania, USA.

[2]Department of Genetics, Perelman School of Medicine, University of Pennsylvania, Philadelphia, Pennsylvania, USA.

[3]Department of Physiology, Perelman School of Medicine, University of Pennsylvania, Philadelphia, Pennsylvania, USA.

[4]Department of Medicine, Perelman School of Medicine, University of Pennsylvania, Philadelphia, Pennsylvania, USA.

*Correspondence:

Jonathan Epstein

602 South Tower, PCAM

3400 Civic Center Blvd.

Philadelphia, PA 19104

1 (215) 898-8731

epsteinj@pennmedicine.upenn.edu

Rajan Jain

Smilow Center for Translational Research

3400 Civic Center Blvd., Room 09-102

Philadelphia, PA 19104

1 (215) 573-3011

jainr@pennmedicine.upenn.edu

Abstract

Cell-type-specific 3D organization of the genome is unrecognizable during mitosis. It remains unclear how essential positional information is transmitted through cell division such that a daughter cell recapitulates the spatial genome organization of the parent. Lamina-associated domains (LADs) are regions of repressive heterochromatin positioned at the nuclear periphery that vary by cell type and contribute to cell-specific gene expression and identity. Here we show that histone 3 lysine 9 dimethylation (H3K9me2) is an evolutionarily conserved, specific mark of nuclear peripheral heterochromatin and that it is retained through mitosis. During mitosis, phosphorylation of histone 3 serine 10 temporarily shields the H3K9me2 mark allowing for dissociation of chromatin from the nuclear lamina. Using high-resolution 3D immuno-oligoFISH, we demonstrate that H3K9me2-enriched genomic regions, which are positioned at the nuclear lamina in interphase cells prior to mitosis, re-associate with the forming nuclear lamina before mitotic exit. The H3K9me2 modification of peripheral heterochromatin ensures that positional information is safeguarded through cell division such that individual LADs are re-established at the nuclear periphery in daughter nuclei. Thus, H3K9me2 acts as a 3D architectural mitotic guidepost. Our data establish a mechanism for epigenetic memory and inheritance of spatial organization of the genome.

Introduction

In order for a dividing cell of a given lineage to maintain its identity, it must pass along to its progeny not only a complete copy of its genome, but also the memory of its specific cellular identity (Buchwalter et al., 2019, Towbin et al., 2013, Amendola and van Steensel, 2014). It is well appreciated that the spatial arrangement of the genome inside the nucleus contributes to regulation of cell-fate choices and differentiation (Peric-Hupkes et al., 2010, Phillips-Cremins et al., 2013). However, the mechanistic underpinnings of how the blueprint for cell-type-specific nuclear architecture is transmitted from mother to daughter cells in order to maintain cell identity remain poorly understood (Dekker et al., 2017).

The chromatin in eukaryotic cells is organized both structurally and functionally into subnuclear compartments (Towbin et al., 2013, Kohwi et al., 2013, Stadhouders et al., 2019) and recent developments in super-resolution microscopy (Cremer et al., 2017, Ricci et al., 2017), chromosome capture methods (Dekker et al., 2002, Dekker et al., 2013), and chromatin immunoprecipitation (ChIP) (Collas, 2010, Kubben et al., 2010) have greatly increased our understanding of 3D nuclear architecture (Naumova et al., 2013). Separation of transcriptionally active and inactive chromatin in three-dimensional space reinforces efficient regulation of gene expression and maintains silencing of heterochromatic loci (reviewed in (Andrey and Mundlos, 2017, Buchwalter et al., 2019, Amendola and van Steensel, 2014, Bickmore, 2013)). This is illustrated by examples of aberrant gene expression patterns that occur upon disruption of topological domains and, in extreme cases, are associated with oncogenic transformation (Andrey and Mundlos, 2017, Flavahan et al., 2016). Heterochromatin is segregated into spatially distinct subnuclear compartments including peripherally located lamina-associated domains (LADs) (Guelen et al., 2008), which encompass approximately 30-40% of the genome (Peric-Hupkes et al., 2010, Poleshko et al., 2017). Multiple examples in mammalian cell types indicate that proper positioning of LADs contributes to cell-type-specific gene expression (Peric-Hupkes et al., 2010, Poleshko et al., 2017, Robson et al., 2016). Likewise, in Drosophila, competence of neuroblasts to respond to inductive signals depends upon stage-specific reorganization of peripheral heterochromatin (Kohwi et al., 2013), and muscle differentiation in *Caenorhabditis elegans* requires anchoring of heterochromatin to the nuclear periphery (Gonzalez-Sandoval et al., 2015). These findings, combined with the observation that many developmental and lineage-specific genes reside in LADs, suggests a key role for peripheral heterochromatin in establishment and

maintenance of cellular identity (Zullo et al., 2012, Poleshko et al., 2017, Peric-Hupkes et al., 2010). LADs are defined by their interaction with the nuclear lamina which is disassembled during cell division, posing a conundrum as to how cell-type specific LADs are remembered through mitosis.

The molecular mechanisms by which LADs are established and maintained at the nuclear periphery remain poorly understood. For example, there does not appear to be a clear targeting sequence that localizes areas of the genome to the nuclear periphery (Zullo et al., 2012, Meuleman et al., 2013). However, histone post-translational modifications have been implicated in LAD regulation. Proline Rich Protein 14 (PRR14) has been shown to recognize H3K9me3, found on both peripheral and nucleoplasmic heterochromatin, through an interaction with HP1 (Poleshko et al., 2013). In addition, work from our group and others has demonstrated a specific enrichment for H3K9me2 at the nuclear periphery, raising the possibility of a regulatory role in LAD positioning (Poleshko et al., 2017, Kind et al., 2013). CEC-4, a *C. elegans* chromodomain-containing protein, localizes to the nuclear periphery and has been shown to be a reader of H3K9 methylated chromatin (Gonzalez-Sandoval et al., 2015). Depletion studies using RNAi and loss-of-function mutants demonstrated that CEC-4 is required for peripheral heterochromatin anchoring but not transcriptional repression. While not all of the tethering complexes and molecular determinants responsible for the interaction of heterochromatin with the nuclear lamina have been determined, it is clear that these associations must be disrupted upon mitotic entry when the nuclear envelope breaks down and the chromosomes condense. Furthermore, these interactions must be precisely re-established upon mitotic exit when the cell reforms an interphase nucleus.

Entry into mitosis involves eviction of proteins, including RNA polymerase and many transcription factors, and reorganization of chromosomes into their characteristic metaphase form (Naumova et al., 2013). Remarkably, at mitotic exit, cell-type-specific chromatin architecture, transcription factor binding, and gene expression are re-established (reviewed in (Oomen and Dekker, 2017, Palozola et al., 2019, Hsiung and Blobel, 2016, Probst et al., 2009, Festuccia et al., 2017)). While both interphase nuclear architecture and post-mitotic restoration of transcription factor association with the genome have been extensively studied (Palozola et al., 2019, Kadauke and Blobel, 2013), our understanding of how cell-type-specific genome organization including LADs is restored in daughter cells after mitosis is less well developed.

Pioneering studies in the 1980s revealed the necessity for DNA in the process of nuclear lamina reassembly after mitosis, and the activity of kinases and phosphatases were implicated in mediating interactions between lamin and chromosomes (Foisner and Gerace, 1993, Newport, 1987, Burke and Gerace, 1986, Gerace and Blobel, 1980), although the mechanistic explanation for the dependence of reassembly on chromatin has been unclear. Here, we utilize high resolution, single-cell imaging and oligopaints to simultaneously track 82 LAD and non-LAD genomic loci through mitosis. We show that the H3K9me2 modification of nuclear lamina-associated heterochromatin, revealed upon dephosphorylation of H3S10 at mitotic exit, provides a 3D spatial guidepost for genomic regions that are to be re-localized to the nuclear periphery following mitosis and that the nuclear lamina of daughter cells reassembles around the exposed H3K9me2 mark.

Results

H3K9me2 is an evolutionarily conserved mark of peripheral heterochromatin

Heterochromatin is organized in multiple compartments throughout the nucleus (Pueschel et al., 2016), and H3K9me2 is a posttranslational histone modification that specifically marks heterochromatin at the nuclear periphery (Poleshko et al., 2017). Immunostaining of murine NIH/3T3 fibroblasts for repressive histone modifications demonstrates the distribution of the major types of heterochromatin in the nucleus of a single cell (Figure 1a). H3K9me2 marks only peripheral heterochromatin, whereas H3K9me3 and H3K27me3 co-localize with heterochromatin in the nuclear interior, or at both the interior and the periphery (Figure 1a, Figure S1). The close association between H3K9me2 and Lamin B in single cell immunostaining is consistent with the correlation between H3K9me2 and Lamin B ChIP-seq data (Figure S1). The adjacency of H3K9me2 chromatin to the nuclear lamina was verified by super-resolution microscopy (Figure 1b). Stochastic Optical Reconstruction Microscopy (STORM) using a Voronoi tessellation confirms a non-random distribution of the H3K9me2 signal at the periphery of the nucleus (Figure S2). We further examined H3K9me2-marked heterochromatin across species and observe that restriction to the nuclear periphery is evolutionarily conserved from *C. elegans* to humans (Figure 1c) suggesting functional significance of the localization of this histone post-translational modification.

Figure 1

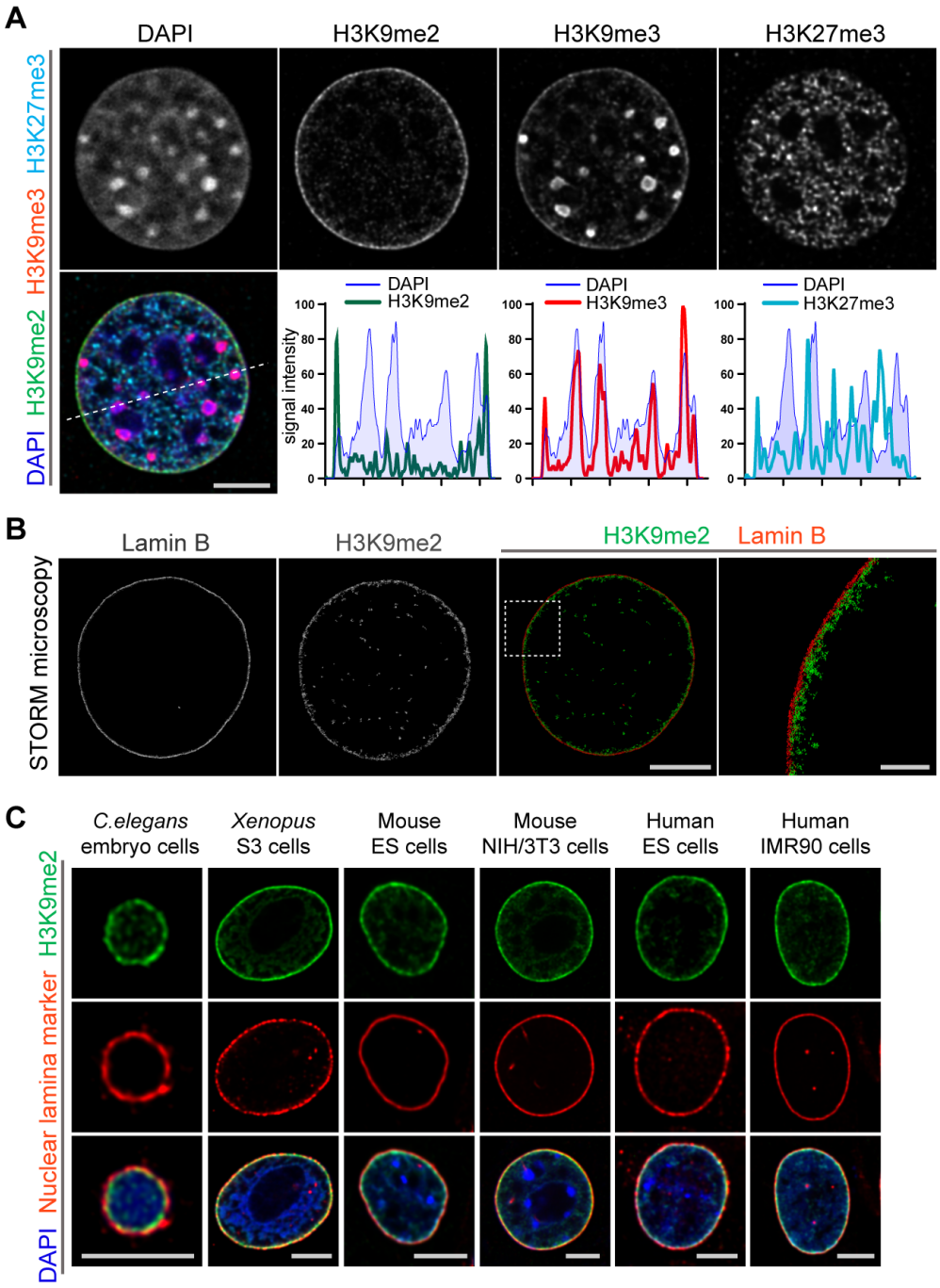

Figure 1. Localization of H3K9me2-marked chromatin at the nuclear periphery is evolutionarily conserved. (A) Immunofluorescent confocal images illustrating localization of the indicated repressive chromatin marks in the nucleus of a NIH/3T3 cell, counterstained with DAPI; dashed line indicates position of the line signal intensity profiles. Scale bar: 5μm **(B)** Representative super-resolution images of a NIH/3T3 cell stained for H3K9me2 and Lamin B obtained using Stochastic Optical Reconstruction Microscopy (STORM). Scale bar: 5μm **(C)** Localization of H3K9me2-marked chromatin in distinct species, co-stained with nuclear lamina markers (Lamin 1 for *C. elegans*; Lamin B all others), counterstained with DAPI. Scale bars: 5μm.

Previously, distinctions between genomic regions marked by H3K9me2 versus H3K9me3 were unclear, perhaps because of lack of specificity of relevant antibodies. Therefore, we extensively characterized the specificity of the H3K9me2 antibody employed in these studies (Figure 2). By preincubating the anti-H3K9me2 antibody with peptides representing each of the possible histone tail modifications before use in immunostaining, we were able to determine that the H3K9me2 antibody detects only the dimethyl modification and only on lysine 9 of histone H3 (Figure 2a). Additionally, by blocking the H3K9me2 antibody with an H3K9me2 peptide, the specific signal observed at the nuclear periphery can be distinguished from non-specific background signal observed in the nuclear interior and detected with signal intensity analysis (Figure 2b). This observation was further confirmed by STORM imaging (Figure 2c).

Figure 2

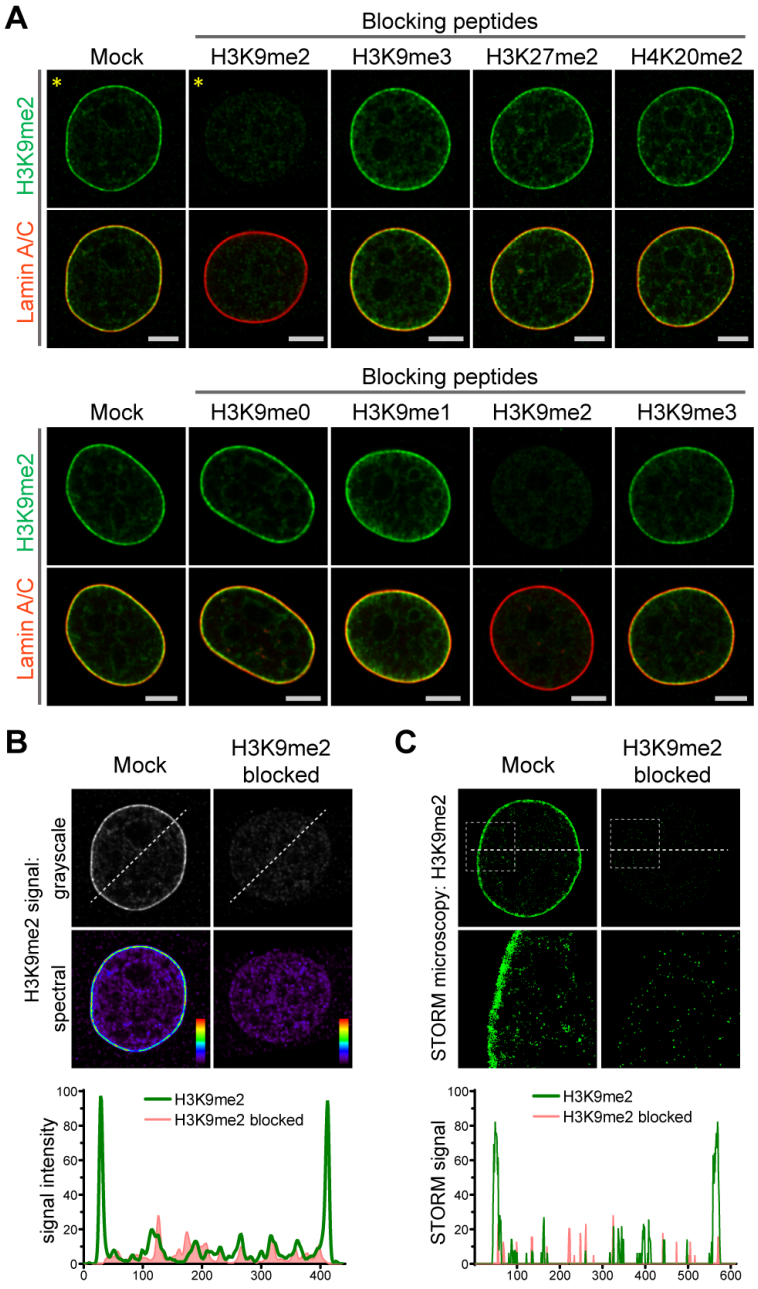

112

113 **Figure 2. Anti-H3K9me2 antibody used in immunofluorescence assays is specific**. **(A)** Mouse C2C12
114 cells stained with nuclear marker Lamin A/C and H3K9me2 antibodies preincubated with indicated
115 blocking peptides. **(B)** Highlighted images (*) from panel A, displayed in grayscale and signal intensity
116 spectral view; line signal intensity profile illustrates H3K9me2-specific signal (green) and non-specific
117 antibody background (red). **(C)** STORM images of NIH/3T3 cell stained for H3K9me2 and blocked with
118 mock or H3K9me2 peptide; line signal intensity profile below as in panel B.

H3K9me2 is required for nuclear peripheral localization of chromatin

Given the specificity of H3K9me2 for peripheral heterochromatin, we hypothesized that this epigenetic histone modification is necessary for peripheral localization of chromatin and might be recognized by a nuclear peripheral protein "reader" to tether chromatin to the nuclear lamina (Figure 3a). In *C. elegans,* CEC-4 functions as a reader of methylated H3K9 and is localized to the nuclear periphery where it is thought to function as part of a tethering complex for peripheral heterochromatin (Gonzalez-Sandoval et al., 2015). Mammalian functional orthologues of CEC-4 have not yet been identified. Since CEC-4 is required for peripheral heterochromatin anchoring (Gonzalez-Sandoval et al., 2015), we compared the localization of H3K9me2 in wild-type and *cec-4*-null embryo cells. Immunostaining revealed a dramatic alteration in spatial patterning in which H3K9me2 is no longer restricted to the periphery in *cec-4*-null cells (Figures 3b and 3c). Localization of the H3K9me2-marked chromatin at the nuclear lamina was restored by expression of the CEC-4-mCherry transgene (Figure 3c, Figure S3). Loss of CEC-4 does not have the same effect on H3K9me3. H3K9me3 is found both at the nuclear periphery and in the nucleoplasm, but its localization does not vary between wide-type and *cec-4*-null embryo cells (Figure S3). These data suggest loss of a peripheral heterochromatin tether, CEC-4, results in a specific effect on H3K9me2-marked chromatin and not H3K9me3-marked chromatin.

To extend our results and probe the role of H3K9 in chromatin positioning in mammalian cells, we expressed GFP-tagged histone H3 (hereafter H3) or GFP-tagged mutant forms of H3 in which Lys9 was substituted with alanine (H3K9A) or glutamic acid (H3K9E); both substitutions preclude methylation at this position in H3. GFP-tagged proteins were expressed in NIH/3T3 cells at relatively low levels compared to endogenous H3 (Figure S4) and attempts to drive higher levels of expression resulted in cell death. Wild-type GFP-H3 was observed throughout the nucleus including at the nuclear periphery, where it overlapped with endogenous H3K9me2 staining, immediately adjacent to Lamin B (Figure 3d). In contrast, GFP-H3K9A and GFP-H3K9E failed to partition to the nuclear periphery (Figures 3d-f). This indicates that H3K9, or a residue at this position that can be methylated, is necessary for peripheral localization of H3. Combined with the CEC-4 results, this suggests that dimethylation of H3K9 orchestrates positioning of chromatin to the nuclear periphery.

Figure 3

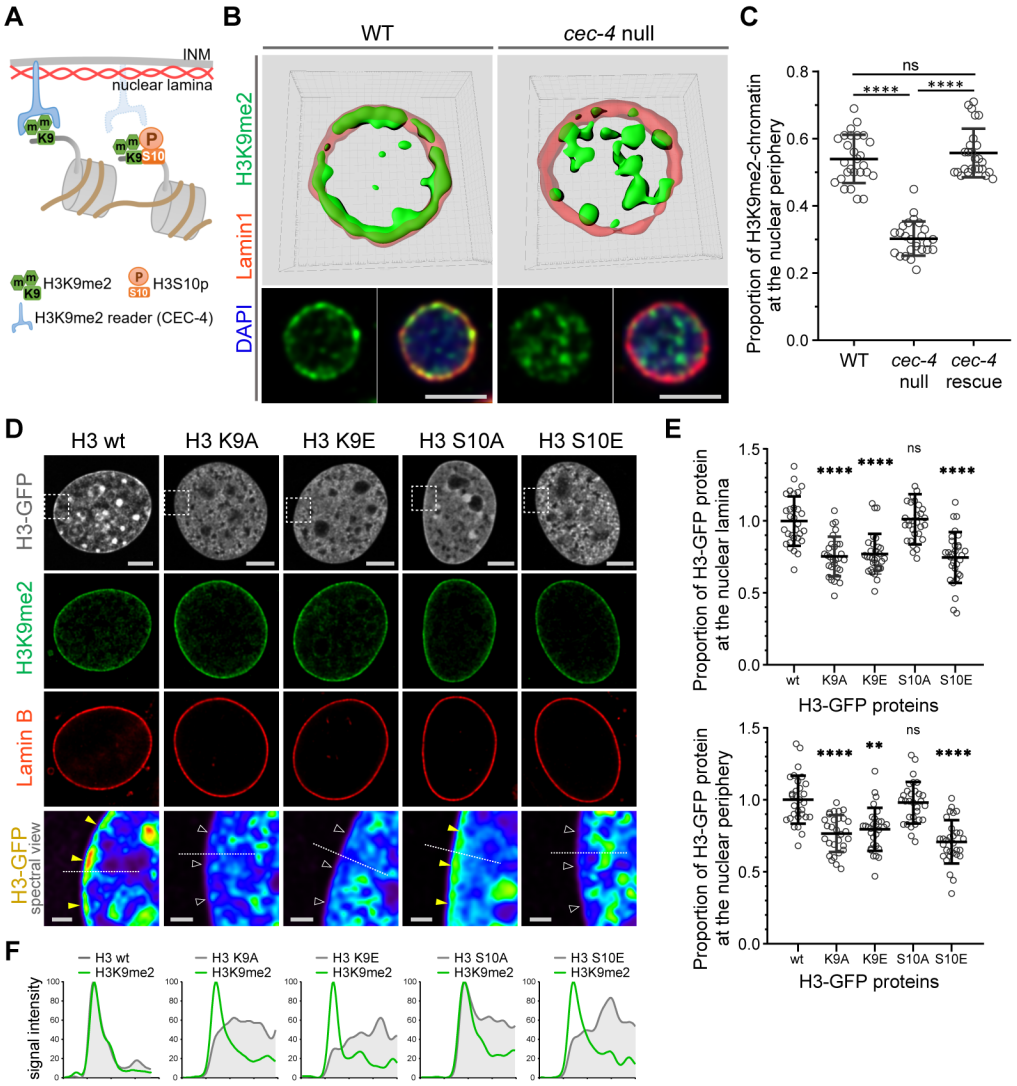

Figure 3. H3K9me2 is essential for histone H3 positioning at the nuclear periphery. (A) Schematic illustrating *C. elegans* protein CEC-4 tethering H3K9me2-marked chromatin to the nuclear periphery; INM: inner nuclear membrane. **(B)** Localization of H3K9me2-marked chromatin (green) in wild-type (WT) and *cec-4*-null *C. elegans* embryo cells, counterstained with Lamin 1 (red) and DAPI (blue); 3D reconstruction (top); immunofluorescent confocal images of *C. elegans* embryo cells (bottom). Scale bars: 3µm **(C)** Dot plot of the proportion of total H3K9me2-marked chromatin at the nuclear lamina in WT, *cec-4*-null, and *cec-4*-rescued embryo cells (mean±SD); n=25 cells per condition. **(D)** Localization of indicated histone H3-GFP fusion proteins in NIH/3T3 cells; counterstained with H3K9me2 (green) and Lamin B (red); spectral views (magnifications of top panels as indicated by dashed squares) illustrate H3-GFP signal intensity. Localization of the H3-GFP at the nuclear periphery (yellow arrowheads) or loss of peripheral localization (white arrowheads). Scale bars: 5µm (top panels) and 1µm (bottom panels). **(E)** Dot plot of the proportion of indicated H3-GFP fusion protein at the nuclear lamina (marked by Lamin B, top) or within the layer of peripheral heterochromatin (marked by H3K9me2, bottom), normalized to wt H3-GFP, calculated using Lamin B or H3K9me2 signal as a mask (mean±SD); n=30 cells per condition. **(F)** Line signal intensity profiles of corresponding images in panel D indicated by dashed lines. Statistical analyses performed using one-way ANOVA non-parametric Kruskal-Wallis test; **** p<0.0001, **p=0.0024, ns: not significant.

A phospho-methyl switch controls peripheral heterochromatin localization

H3S10 phosphorylation is associated with mitotic chromosome condensation (Wei et al., 1999, Prigent and Dimitrov, 2003) and, together with the neighboring Lys9 residue, has been proposed to function as a 'phospho-methyl switch' to modulate binding of H3 to effector proteins (Varier et al., 2010, Fischle et al., 2003, Wang and Higgins, 2013). Expression of a GFP-tagged H3 mutant in which Ser10 is replaced with the phospho-mimic glutamic acid (H3S10E) resulted in distribution of the GFP-H3S10E throughout the nucleus, but notably not at the nuclear periphery (Figures 3d-f). This is consistent with the ability of phosphorylated Ser10 to inhibit interaction of the reader with H3K9me2 and suggests that phosphorylation of Ser10 can prevent H3 peripheral localization. Replacement of H3 Ser10 with an alanine (H3S10A) precludes phosphorylation at this site and did not disrupt peripheral localization. Instead, H3S10A produced a pattern similar to wild-type GFP-H3 in interphase cells (Figures 3d-f). These results suggest that H3K9me2 is required for localization of heterochromatin to the nuclear periphery. Further, they indicate that phosphorylation of Ser10 can prevent or disrupt this association as part of a phospho-methyl switch.

H3K9me2 persists through mitosis and associates with reassembling nuclear lamina in daughter cells at mitotic exit

Given the requirement for H3K9me2 to position heterochromatin at the nuclear lamina in interphase, we asked whether the H3K9me2 mark is maintained through cell division or if the histone modification is lost and re-acquired *de novo* in daughter cells. Examination of cells progressing through the consecutive phases of mitosis revealed persistence of H3K9me2 on mitotic chromatin (Figure 4a). Prior to disassembly of the nuclear lamina in prophase, H3K9me2-marked chromatin begins to detach from the nuclear periphery. Concordant with this detachment, we observe phosphorylation of Ser10 on the H3 tail adjacent to dimethylated Lys9 (H3K9me2S10P) beginning in prophase and persisting until late telophase (Figures 4a and 4b). As for the anti-H3K9me2 antibody, we carefully tested the specificity of the anti-H3K9me2S10P antibody used in these experiments and verified that it does not recognize the H3K9me2 epitope without an adjacent phosphate group on S10 (Figure S5). H3S10 phosphorylation in prophase may

197 contribute to release of H3K9me2 readers/tethers (Eberlin et al., 2008, Hirota et al., 2005) and
198 detachment from the nuclear periphery.

199 We also examined cells at successive points in telophase. As telophase progresses, re-
200 establishment of the H3K9me2 layer occurs in parallel with reassembly of the nuclear lamina. We
201 observed aggregation of H3K9me2-marked chromatin and the reformation of this heterochromatin
202 layer at the interface with the newly forming nuclear lamina structure (Figure 4c). However,
203 chromatin marked with H3K9me2S10P was not enriched at the interface of the forming nuclear
204 lamina but remained in the nucleoplasm (Figure 4d), suggesting that loss of S10 phosphorylation
205 occurs prior to association of chromatin with the nuclear lamina. We detected little or no
206 H3K9me2S10P in daughter cells after mitosis was complete (Figure 4d).

207 A subset of H3K9me3-marked chromatin is at the nuclear periphery, though it is not restricted to
208 the periphery as is H3K9me2. H3K9me3 is enriched in microsatellite heterochromatin and persists
209 through mitosis (Figure 5a). In addition, in telophase we noted strong differences in localization
210 of other repressive (H3K9me3, H3K27me3) and active (H3K4me3) histone marks in contrast to
211 H3K9me2 (Figure 5b). Trimethylated H3K9 is also distinct from H3K9me2 in that H3K9me3
212 chromatin is not enriched at the interface with the forming nuclear lamina during telophase and
213 mitotic exit. In the newly formed daughter cells, we observed H3K9me2- but not H3K9me3-
214 marked chromatin preferentially associated with the nuclear lamina.

215

Figure 4

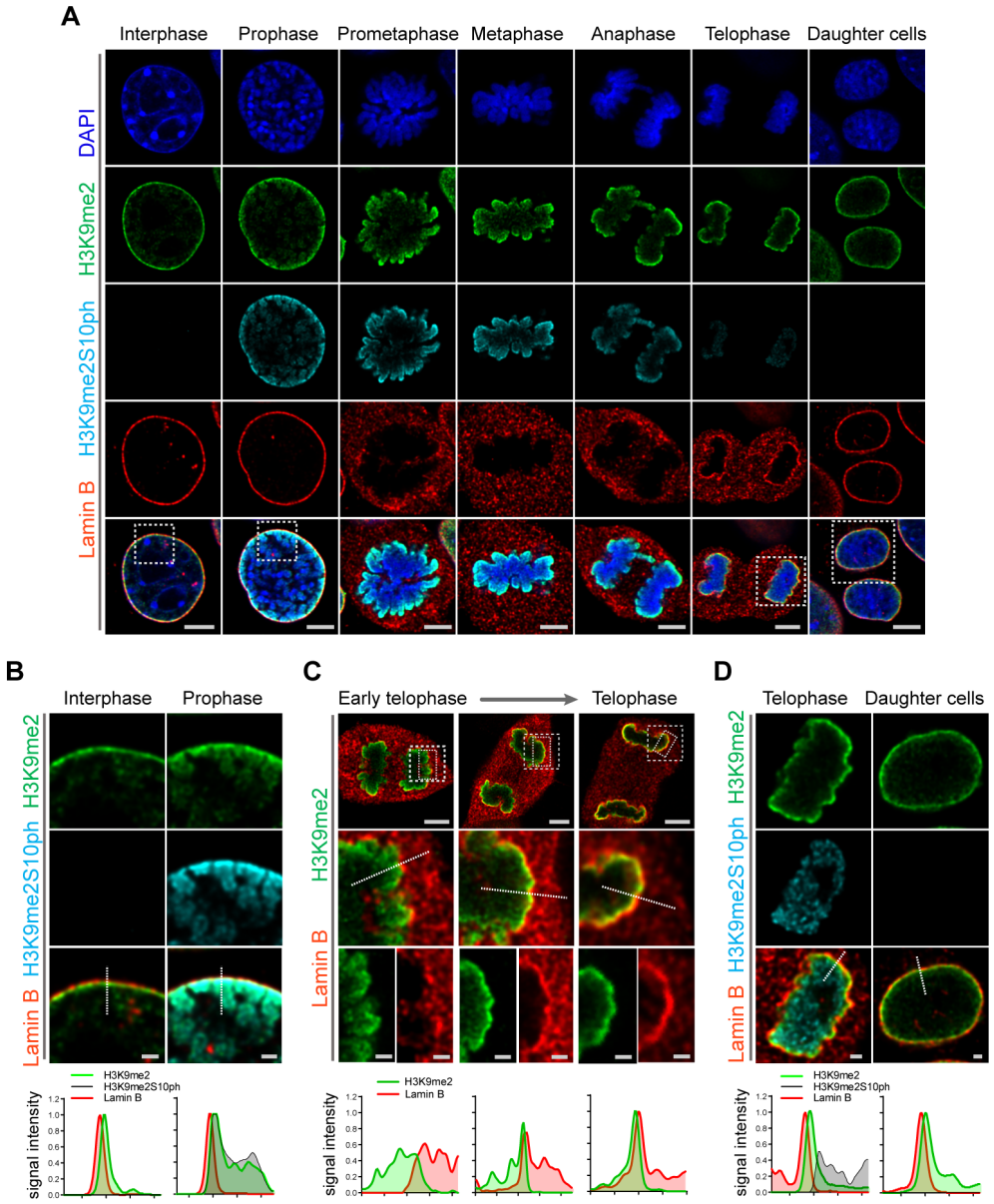

Figure 4. H3K9me2-marked chromatin is maintained throughout mitosis to be re-established at the nuclear lamina during nuclear lamina reassembly. (A) Immunofluorescent confocal images of mouse C2C12 cells illustrating localization of H3K9me2- and H3K9me2S10ph-marked chromatin and Lamin B during different stages of mitosis; DNA visualized with DAPI. Scale bars: 5μm. **(B)** Magnified images of Interphase and Prophase from panel (A) demonstrating detachment of the H3K9me2-chromatin from the nuclear lamina concomitant with H3K9me2S10ph phosphorylation; scale bar: 1μm. **(C)** Representative images of cells progressing through telophase as the layer of peripheral H3K9me2-marked heterochromatin (green) is re-established and nuclear lamina (Lamin B, red) is reassembled; dashed boxes in top panels indicate higher resolution images. Scale bars: 5μm (top) and 1μm (bottom panels). **(D)** Magnified images of telophase and daughter cells from panel A demonstrating de-phosphorylated H3K9me2-chromatin (green) assembled at the nuclear lamina (Lamin B, red), while the phosphorylated form (H3K9me2S10ph, cyan) remains localized in the nuclear interior; scale bar: 1μm. Dashed lines indicate location of corresponding line signal intensity profiles (bottom row).

Figure 5

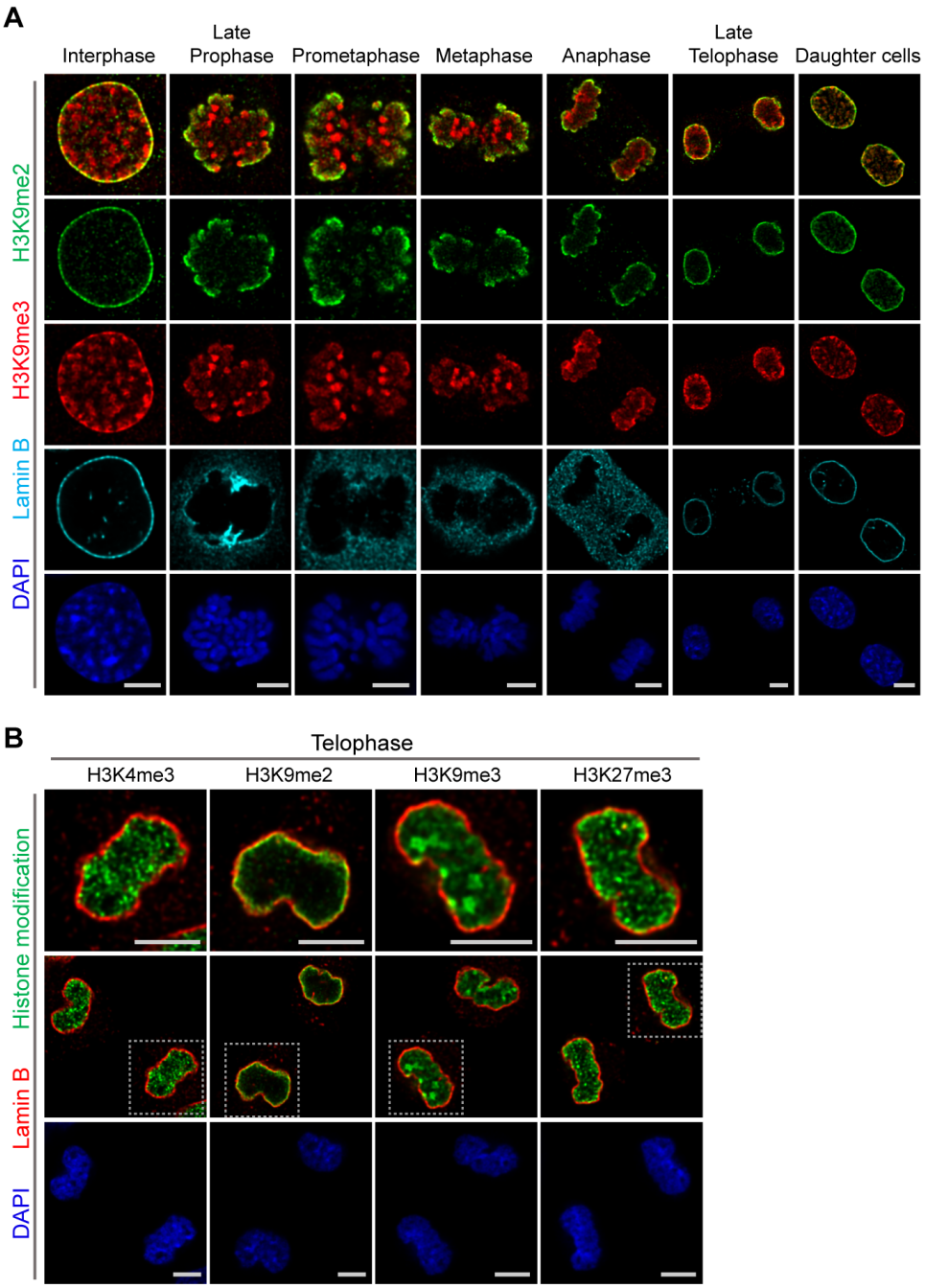

Figure 5. Localization of H3K9me2- and H3K9me3-marked chromatin differs during mitosis. (A) Representative immunofluorescent confocal images illustrating a difference in localization of H3K9me2 (green) and H3K9me3 (red) chromatin marks in interphase, during mitosis, and upon mitotic exit; co-stained with Lamin B (cyan) and DAPI (blue). **(B)** Representative immunofluorescent confocal images of telophase cells illustrating difference in localization of different histone modifications (green) in relation to Lamin B (red); co-stained with DAPI (blue). Dashed boxes in middle panels indicate higher resolution images. Scale bars: 5μm.

Specific LADs positioned at the nuclear periphery prior to mitosis re-associate with forming nuclear lamina in telophase

Restoration of H3K9me2-marked chromatin at the nuclear lamina prior to mitotic exit suggests a mechanism for inheritance of spatial localization of specific genomic loci within the peripheral heterochromatin layer. Our experiments thus far demonstrate that H3K9me2-marked chromatin, in general, is re-established at the nuclear lamina. Conflicting reports have emerged regarding whether LADs are reshuffled at every cell division to stochastically localize in other, non-lamina-associated heterochromatic subcompartments (Kind et al., 2013, Zullo et al., 2012, Kind et al., 2015). To determine whether specific genomic regions are re-established at the nuclear periphery at mitotic exit, we used fluorescence *in situ* hybridization (FISH)-based imaging to monitor the localization of individual genomic regions in single cells. We designed libraries of fluorescent DNA oligo probes (oligopaints) targeting domains of the genome that were identified through population-based studies (Meuleman et al., 2013, Peric-Hupkes et al., 2010, Poleshko et al., 2017) to be either cell-type invariant regions of nuclear peripheral, H3K9me2-marked heterochromatin (LADs) or cell-type invariant regions of euchromatin (non-LADs). The pool of probes (41 LAD and 41 non-LAD regions) includes regions from every mouse autosome (Figure S6, Table S1). We performed immunofluorescent in situ hybridization with the probes in individual cells in interphase and mitosis; reconstruction of stacks of confocal images allowed us to visualize the 3D position of specific genomic loci (Movies S1-S3).

In a population of interphase cells, we found the LAD probes to be at the periphery of individual nuclei at a frequency consistent with previous observations of haploid cells in studies using single-cell DamID (Kind et al., 2015). An average of 82% of LAD probes (74-90% in individual cells) were positioned at the nuclear periphery within the measured thickness of the H3K9me2 chromatin layer in interphase cells (Figure 6a, Movie S1). Non-LAD probes, assessed in each of the same interphase cells, were more frequently found in the nucleoplasm, as expected: an average of 89% of non-LAD probes (79-95% in individual cells) segregated outside of the peripheral chromatin layer (Figure 6a).

Next, we examined the location of these representative LAD and non-LAD genomic loci in cells undergoing mitosis. Both LAD and non-LAD probes are present at similar distances from the DNA surface in cells in metaphase, a point in mitosis at which the nuclear lamina has dissembled (Figure

6b, Movie S2). However, by telophase, LAD probes have repositioned to the nuclear periphery (Figure 6c, Movie S3), indicating that H3K9me2-marked domains that were at the periphery in parent cells are specifically repositioned at the periphery in daughter nuclei before mitotic exit. In these same cells in telophase, non-LAD probes remained largely in the nucleoplasm, away from the nuclear lamina (Figure 6c, Movie S3). Thus, specific LADs found at the nuclear periphery in parental cells are repositioned at the periphery at mitotic exit.

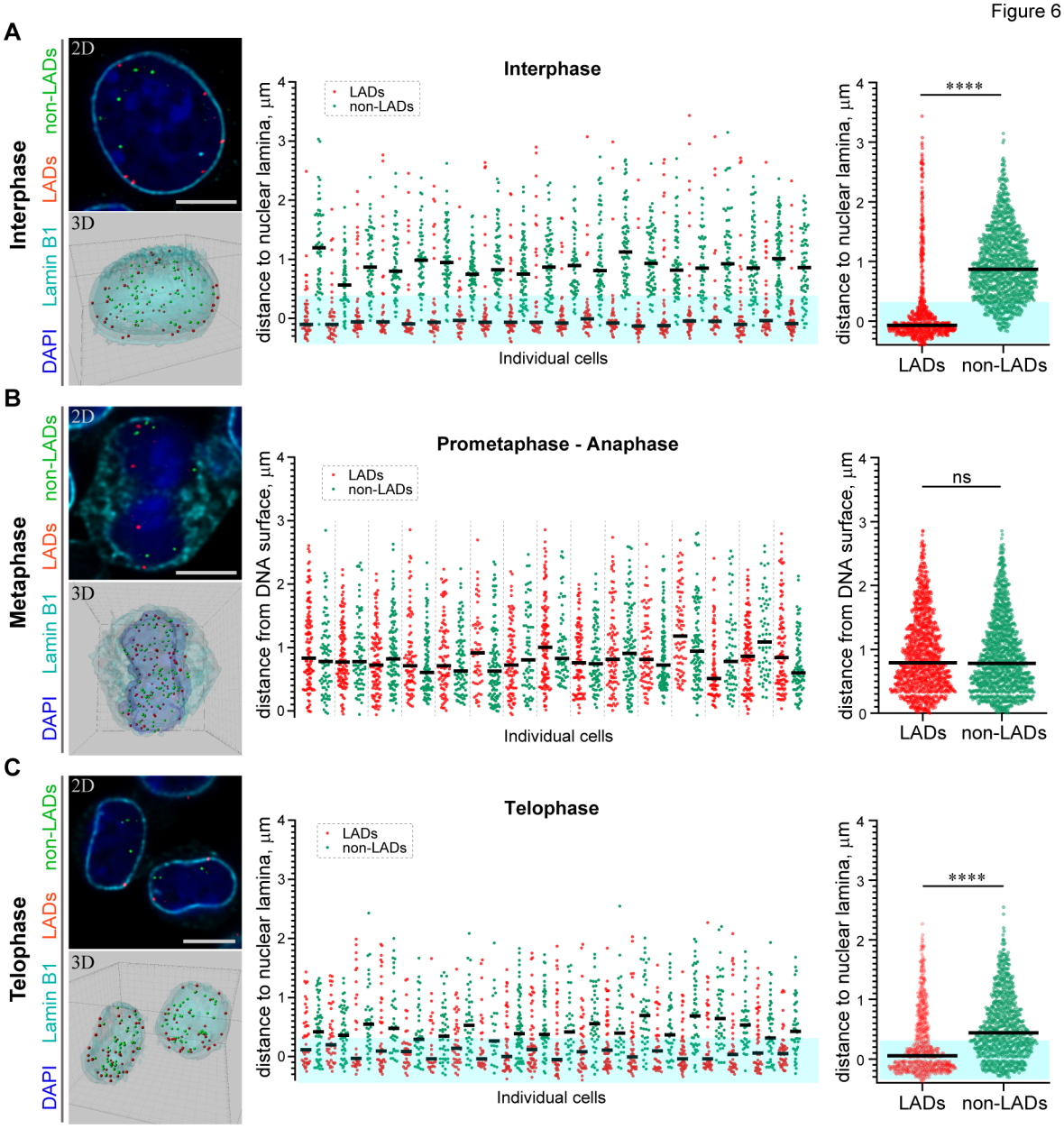

Figure 6. H3K9me2-enriched LADs are positioned at the nuclear lamina in interphase cells and the position is inherited through mitosis. (A) Localization of LADs and non-LADs in interphase mESCs. Left panels show representative immuno-FISH image (top) and 3D image reconstruction (bottom) of cells hybridized with fluorescent DNA oligopaint probes targeting individual LADs (red) and non-LADs (green), and immunostained for Lamin B1 (cyan) and DAPI (blue). Scale bar: 5µm. Dot plots show distribution and median of distances to the nuclear periphery of individual LAD and non-LAD probes for individual cells (middle) and cumulative over all cells (right) in interphase. **(B)** As in panel A for prometaphase-metaphase-anaphase cells. **(C)** As in panel A for telophase cells. For dot plots, nuclear periphery defined by Lamin B1 or DNA edge; black line: median value; cyan boxes indicate average thickness of H3K9me2 peripheral heterochromatin layer. n≥20 individual nuclei; N=870-1399 individual LADs or non-LADs per condition. Statistical analysis performed using two-tailed t-test; **** $p<0.0001$; ns: not significant.

Discussion

Our results provide experimental support of a model for nuclear peripheral localization and mitotic inheritance of lamina-associated heterochromatin (Figure 7). We show that H3K9me2 marks chromatin domains that are specifically positioned at the nuclear lamina during interphase. In mitosis, these domains retain and are bookmarked by H3K9me2. H3S10 phosphorylation promotes release from the nuclear periphery, likely by masking the Lys9 dimethyl modification from recognition by its reader/tether (Fischle et al., 2003, Wang and Higgins, 2013, Eberlin et al., 2008). In late stages of mitosis, dephosphorylation of H3S10 unmasks bookmarked LADs which are then reassembled at the nuclear periphery during nuclear lamina reformation in the nuclei of daughter cells.

Figure 7

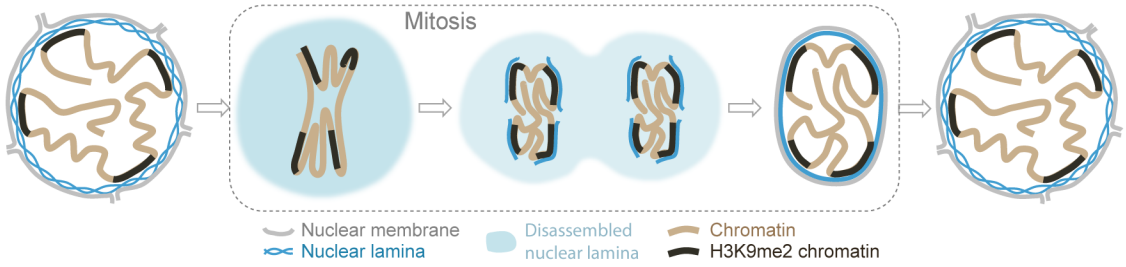

Figure 7. Model illustrating the role of the H3K9me2 chromatin modification in inheritance of peripheral heterochromatin localization through cell division.

How cells convey information related to cellular identity to daughter cells has been a long-standing focus of investigation. Although mitotic chromosomes are condensed and transcriptionally silent, it is now appreciated that many nuclear factors remain associated with specific regions of mitotic chromatin, and some histone post-translational modifications are also retained. The concept of "mitotic bookmarking" has been put forth to describe mechanisms by which transcriptionally active regions of euchromatin may be "remembered" and rapidly re-activated upon mitotic exit (Kadauke and Blobel, 2013, Palozola et al., 2019, Sureka et al., 2018). Here, we extend this concept by elucidating a mechanism for transmitting a blueprint of the 3D organization of the genome from mother to daughter cell with a specific focus on peripheral heterochromatin associated with the inner nuclear lamina. Our data indicate that H3K9me2 acts as a 3D architectural mitotic guidepost.

Our data highlight the role of H3S10 phosphorylation adjacent to dimethylated Lys9 in 3D mitotic bookmarking, allowing for dissociation of peripheral heterochromatin from the nuclear lamina while retaining memory of genomic regions that will be reattached to the newly formed nuclear lamina upon dephosphorylation and mitotic exit. This example of a phospho-methyl switch extends previous studies that implicated related phospho-methyl switch mechanisms in transcriptional bookmarking without invoking regulation of 3D genome organization or nuclear reassembly. For example, H3S10 phosphorylation can displace HP1 binding to trimethylated Lys9 during mitosis (Hirota et al., 2005, Fischle et al., 2005). In another example, the active histone mark H3K4me3 is bound by TFIID and the basal transcriptional machinery during interphase. While H3K4me3 is maintained through mitosis, phosphorylation of Thr3 results in dissociation of TFIID and transcriptional silencing. The retention of H3K4me3 is thought to allow for rapid re-initiation of transcription after mitosis when Thr3 is dephosphorylated (Varier et al., 2010, Sawicka and Seiser, 2014). Our results supporting an H3K9me2S10 phospho-methyl switch suggest that this conserved mechanism also is employed for mitotic memory of nuclear architecture. During cell division, this mechanism is utilized to release all peripheral heterochromatin from the nuclear lamina, but it will be of interest to determine if a similar process occurs during interphase to release specific LADs from the periphery, perhaps endowing these domains with competence to be accessed by nuclear regulators of transcription. Histone phosphorylation, including H3S10, has been well documented to occur in response to classic signal transduction pathways such as Mapk signaling (Winter et al., 2008) suggesting a potential mechanism for the regulation of LAD release as a component of signal transduction.

The importance of the spatial organization of the genome has attracted increasing attention in recent years with a growing appreciation for unique, lineage-specific LADs and other architectural features. Largescale efforts have focused on characterizing genome organization in interphase, with less attention to how 3D architecture is transmitted through mitosis. Indeed, an early study suggested that LADs might be stochastically formed *de novo* following each cell division rather than inherited from the mother cell following mitosis (Kind et al., 2013). Unless all heterochromatic subcompartments are functionally equivalent, this would be somewhat inconsistent with the role that LADs are thought to play in cell identity (Robson et al., 2016, Peric-Hupkes et al., 2010, Kohwi et al., 2013, Gonzalez-Sandoval et al., 2015, Poleshko et al., 2017). Many reports have documented consistent, cell-type-specific LAD architecture as well as

restoration of particular heterochromatin domains at the lamina after cell division (Zullo et al., 2012, Kind et al., 2015). It is conceivable that cell-type-specific LAD organization is "rediscovered" after mitosis rather than "remembered." But our results, including those produced with LAD-specific oligopaints, indicate that at least a subset of LADs is re-established at the nuclear periphery at the end of mitosis, concomitant with nuclear lamina re-assembly. Thus, a daughter cell inherits the key aspects of 3D chromatin organization required to retain cellular identity.

Mitosis and the period shortly following in G1 may provide a vulnerable period to regulate or modify genome organization. Consistent with this, pioneering experiments artificially tethering areas of the genome to the nuclear lamina noted the requirement for a mitotic event to precede efficient tethering of the genome to the nuclear lamina (Finlan et al., 2008, Reddy et al., 2008, Kumaran and Spector, 2008). Moreover, nuclear transfer experiments demonstrated that mitotic chromatin can be reprogrammed to activate the core pluripotency network 100 times more efficiently than interphase chromatin (Halley-Stott et al., 2014). This may be, in part, because three-dimensional reorganization of the genome after mitosis helps to regulate accessibility. In particular, it is possible that the period during which H3S10 phosphorylation is lost in late mitosis, but before H3K9me2-marked chromatin is fully re-established as lamina-associated heterochromatin at the nuclear periphery, is a particularly vulnerable time to change LAD positioning in daughter cells. Hence, this may also coincide with a window in which cell fate changes associated with modifications in nuclear architecture occur (Gilbert, 2010). This would be in accord with the "quantal theory of differentiation" put forth by Howard Holtzer over 50 years ago which proposed that major steps in lineage determination and cell fate restriction required mitotic events (Holtzer et al., 1972).

Classic cell biology experiments have demonstrated the necessity of kinase-phosphatase activity for mitotic progression and the requirement for chromatin to allow nuclear membranes to reform in daughter cells after mitosis (Gerace and Blobel, 1980, Newport, 1987, Foisner and Gerace, 1993, Burke and Gerace, 1986, Wei et al., 1999, Prigent and Dimitrov, 2003, Wandke and Kutay, 2013, Haraguchi et al., 2008). Our model provides a mechanistic explanation for these requirements and advances current models of mitotic bookmarking by introducing the concept of 3D architectural mitotic bookmarking. This model for epigenetic inheritance may have implications for understanding how cells adopt new fates in the setting of asymmetric cell

376 divisions, and how cellular identity may be lost or altered in the context of cancer or trans-
377 differentiation. For example, it will be of great interest to determine if the re-establishment of
378 spatial chromatin organization is disrupted in cells as they undergo oncogenic transformation
379 and/or cellular reprogramming.

380

Author Contributions

A.P., C.L.S., R.J., and J.A.E. conceived of the project and designed experiments. A.P. performed experiments. P.S. and J.I.M. contributed reagents. C.L.S., S.C.N. and E.F.J. performed oligo probe design and production. M.L. provided algorithms for image analysis. A.P., C.L.S., R.J., and J.A.E. analyzed data and wrote the manuscript. R.J. and J.A.E. supervised the project.

Acknowledgments

We thank Andrea Stout from the Penn CDB Microscopy Core for help with imaging. We thank Matt Good and Nicolas Plachta for discussions and comments on the manuscript. This work was supported by NIH (R35 HL140018 to J.A.E., DP2-HL147123 to R.J., and R35 GM127093 to J.I.M.) and the Cotswold Foundation (to J.A.E.), the WW Smith endowed chair (to J.A.E.), Burroughs Welcome Career Award for Medical Scientists and the Gilead Research Scholars Program (to R.J.). R.J. and J.A.E. received support from the NSF (CMMI-1548571).

Declaration of Interests:

Authors declare no competing interests.

Methods

Cell lines

Murine NIH/3T3 fibroblast and C2C12 skeletal myoblast, and human IMR90 fibroblast cells were maintained at 37ºC in DMEM supplemented with 10% FetalPlex serum complex (Gemini, cat#100-602), penicillin, and streptomycin. Mouse ES cells were maintained at 37ºC on a feeder layer of mitotically inactivated MEFs in DMEM with 15% FBS (Fisher Scientific #SH3007003) and ESGRO LIF (EMD Millipore, cat#ESG1106). Human ES cells were maintained at 37ºC in StemMACS™ iPS-Brew XF media (Miltenyi Biotec GmbH, cat#130-104-368), supplemented with penicillin, and streptomycin. Xenopus S3 cells were maintained at 25oC in 66% L-15 media (Gibco, cat#11415-064) with 10% fetal bovine serum (Atlanta Biologicals, cat#S11550), sodium pyruvate, penicillin, and streptomycin.

Plasmids, mutagenesis and transfection

Expression plasmids for Histone H3-mEmerald was received from Addgene (cat#54115, deposited by Michael Davidson). This plasmid was used to create Histone H3 tail mutant constructs: H3 K9A, H3 K9E, H3 S10A and H3 S10E using QuikChange II XL Site-Directed Mutagenesis Kit (Agilent technologies, cat#200521) according to manufacturer's instruction. Plasmid transfections were performed with FuGENE 6 (Promega, cat#E2691) according to manufacturer instructions. For confocal imaging cells were plated on coverslips (EMS, cat#72204-01), then transfected at 50% confluency and fixed 48 hours post-transfection. Primers used for mutagenesis: H3 K9A (5'-ACTAAACAGACAGCTCGGGCATCCACCGGCGGTAAAGCG, 5'-CGCTTTACCGCCGGTGGATGCCCGAGCTGTCTGTTTAGT); H3 K9E (5'-ACTAAACAGACAGCTCGGGAATCCACCGGCGGTAAAGCG, 5'-CGCTTTACCGCCGGTGGATTCCCGAGCTGTCTGTTTAGT); H3 S10A (5'-ACTAAACAGACAGCTCGGAAAGCCACCGGCGGTAAAGCG, 5'-CGCTTTACCGCCGGTGGCTTTCCGAGCTGTCTGTTTAGT); H3 S10E (5'-ACTAAACAGACAGCTCGGAAAGAAACCGGCGGTAAAGCG, 5'-CGCTTTACCGCCGGTTTCTTTCCGAGCTGTCTGTTTAGT).

C. elegans strains, embryo cell isolation for immunofluorescence

The wild-type strain is N2; the *cec-4* null is deletion strain RB2301 from the Caenorhabditis Genetics Center (CGC); CEC4-mCherry transgene is the GW849 strain (gwSi17 [cec-4p::cec-4::WmCherry::cec-4 3'UTR] II) obtained from Susan Gasser (Gonzalez-Sandoval et al., 2015). The rescue strain was created by crossing *cec-4* mutant [cec-4 (ok3124) deletion] males to GW849 hermaphrodites. Animals were grown as previously described (Stiernagle, 2006). For immunostaining, worms were bleached, then washed off the plate with M9 solution (86mM NaCl, 42mM Na_2HPO_4, 22mM KH_2PO_4, and 1mM Mg_2SO_4, pH 6.5). They were washed with a bleach solution (15ml MilliQ water, 4ml Clorox, and 2ml 5 M KOH) with shaking until adult bodies were dissolved. Then, embryos were washed twice with M9 solution, fixed with 4% formaldehyde solution (incubated at room temperature (RT) for 15 min). Embryos were then flash freeze by immersing tube in an ethanol/dry ice bath for 2 minutes, thawed to RT, and then incubated on ice for 20 min and wash twice with PBS. Fixed embryos were spun on the coverslips at 1000g for 10 min in cushion buffer (100mM KCl, 1mM $MgCl_2$, 0.1mM $CaCl_2$, 10mM HEPES pH7.7, 250mM sucrose, 25% glycerol), then post-fixed with 2% PFA for 10 min at RT. A single-cell suspension of embryonic cells was prepared in a similar manner, but after the beach solution washing step embryos were washed three times in L15 media (Corning Cellgro, cat#10-045-CV), and then incubated in the 0.5mg/ml Chitinase (Sigma, cat#C6137) in Boyd Buffer (25 mM HEPES pH 7.3, 118 mM NaCl, 48 mM KCl, 2 mM $CaCl_2$, 2 mM $MgCl_2$) at RT with rotation/aspiration to dissociate cells. Cells were pelleted at 1000g for 5 min at 4oC and dissolved in PBS. Cells were kept at 4^{o}C before immunostaining.

Immunofluorescence

NIH/3T3 cells, C2C12 cells, undifferentiated mouse and human ES cells, *Xenopus laevis* S3 cells utilized for immunofluorescence experiments were grown on glass coverslips, fixed with 2% paraformaldehyde (PFA) (EMS, cat#15710) for 10 minutes at RT, washed 3 times with DPBS (Gibco, cat#14190-136), then permeabilized with 0.25% Triton X-100 (Thermo Scientific, cat#28314) for 10 minutes. After permeabilization, cells were washed 3 times with DPBS for 5 min, then blocked in 1% BSA (Sigma, cat#A4503) in PBST (DPBS with 0.05% Tween 20, pH 7.4 (Thermo Scientific, cat#28320)) for 30-60 min at RT. Incubated with primary antibodies for 1 hour at RT, then washed three times with PBST for 5 min. Incubated with secondary antibodies for 30-60min at RT, when washed two times with PBST for 5min. Samples were counterstained with

DAPI solution (Sigma, cat#D9542) for 10 min at RT, then rinsed with PBS. Coverslips were mounted on slides using 80% glycerol mounting media: 80% glycerol (Invitrogen, cat#15514-011), 0.1% sodium azide (Sigma, cat#S2002), 0.5% propyl gallate (Sigma, cat#02370), 20mM Tris-HCl, pH 8.0 (Invitrogen, cat#15568-025).

Immunofluorescence and DNA oligo FISH

Mouse ESCs were grown on 0.1% porcine gelatin (Sigma, cat#G2500) coated glass coverslips (EMS, cat#3406), fixed with 2% PFA for 10 minutes at RT. Then cells were immunostained as described above. DNA oligo hybridization protocol was adopted from Rosin et al., 2018 (Rosin et al., 2018). In brief, after incubation with secondary antibodies, samples were washed with DPBS and post-fixed with 2% PFA for 10 minutes at RT, washed 3 times with DPBS and permeabilized with 0.7% Triton X-100 for 10 minutes at RT, then rinsed with DPBS. Incubate coverslips in 70% ethanol, 90% ethanol, and 100% ethanol for 2 minutes each, then incubate in 2X SSC (Corning, cat#46-020-CM) for 5 min. Incubate coverslips in 2X SSCT (2X SSC with 0.1% Tween) for 5 min at RT, then incubate in 2X SSCT with 50% Formamide for 5 min at RT. DNA denaturation was performed in 2X SSCT with 50% Formamide for 2.5 minutes at 92^{o}C, then additional 20 min at 60^{o}C. After DNA denaturation, samples were cooled to RT in humid conditions for 2-3 min, then hybridized with DNA oligo probes in ~50-100 pmol primary DNA probe coverslips were heated at 92^{o}C for 2.5 min on a heat block. Samples were hybridized with DNA oligo probes overnight at 37^{o}C in a humid chamber. After hybridization with primary DNA oligo probes samples were washed in 2X SSCT for 15 min at 60^{o}C, then for 10 min in 2X SSCT for 10 min at RT, then transferred in 2X SSC for 5 min. Next samples were hybridized with a secondary fluorescent DNA oligo probes in dark humidified chamber for 3 hours at RT. Hybridization mix: 10% Formamide, 10% dextran sulfate, 10 pmol secondary DNA probe. After secondary hybridization samples were washed for 5 min in 2X SSCT at 60^{o}C, then 2X SSCT at RT, and 2X SSC buffer with DAPI. Samples were rinsed with DPBS and mounted on a slide.

Image acquisition

All confocal immunofluorescent images were taken using a Leica TCS SP8 3X STED confocal microscope. 3D images were taken as Z-stacks with 0.05µm intervals with a range of 80-250 Z-planes per nucleus. Confocal 3D images were deconvoluted using Huygens Professional software.

Stochastic Optical Reconstruction Microscopy (STORM) images were obtain using Vutara SRX STORM system. Cells for STORM imaging were plated on confocal plates (MatTek, cat#P35GC-1.5-14-C). After immunostaining cells were kept in DPBS until image acquisition. STORM imaging was performed in fresh imaging buffer (50mM Tris-HCl, pH 8.0, 10mM NaCl, 10% (w/v) glucose (Sigma, cat#G8270), 1.5mg MEA (Sigma, cat#30070), 170 AU Glucose oxidase (Sigma, cat#G2133), 1400 AU Catalase (Sigma, cat#C40)). Confocal channel shift alignment and STORM point spread function (PSF) calibration and channel shift alignment were performed using 0.1μm TetraSpeck fluorescent beads (Invitrogen, cat#T7279).

Image analysis

Image analysis were performed using Image J, Imaris 9.0.1, and Vutara SRX software. Representative confocal images show a single focal plane. 2D image analysis was performed using Image J software (National Institute of Health, USA). Line signal intensity profile plots were created using Plot Profile tool. Measurement of localization of the IF signal at the nuclear periphery was performed as a proportion of the signal at the nuclear periphery measured using a mask of the nuclear lamina or H3K9me2 signals, to total signal in the nucleus. 3D image reconstructions were performed using Imaris 9.0.1 software (Bitplane AG, Switzerland) as described (Poleshko et al., 2017). In brief, nuclear lamina, nuclear DNA volume, and H3K9me2-marked chromatin structure were created using Surfaces tool with automatic settings based on the fluorescent signals from the anti-Lamin B, DAPI staining, and anti-H3K9me2 antibodies. DNA oligo FISH probe spots were generated using the Spots tool with a 250nm diameter, created at the intensity mass center of the fluorescent probe signal. Distance from the center of the DNA oligo FISH spot to the edge of the nuclear lamina surface was quantified using the Distance Transformation tool. Thickness of the peripheral heterochromatin layer was calculated as the distance from the H3K9me2 surface inner edge to nuclear lamina inner edge again using the Measurement Points tool. If the distance from the DNA oligo FISH spot to the nuclear lamina was smaller than (or equal to) the average thickness of peripheral chromatin, then the spot was counted as localized to nuclear periphery. In cases when the DNA oligo FISH signal was imbedded into the nuclear lamina layer, the measurement returned negative distances. STORM image and cluster analysis were performed using Vutara SRX software (Bruker, USA) and Voronoi Tessellation Analysis of H3K9me2 STORM images was performed in MATLAB 2016a in a fashion similar to Andronov et al., 2016 (Andronov et al.,

2016). First, the lateral x,y localizations were input into the 'delaunayTriangulation' function, and then used to construct Voronoi polygons using the 'Voronoidiagram' function. Areas of the Voronoi polygons were determined from the vertices with the function 'polyarea'. Multiscale segmentation of the STORM images was carried out using an automatic thresholding scheme in which the thresholds were defined by comparing the Voronoi area distribution of the localizations to a reference distribution of the expected Voronoi areas of random coordinates drawn from a spatial uniform distribution (Levet et al., 2015). The reference distribution was estimated with a Monte-Carlo simulation. The first threshold was selected as $\rho=\delta$, where ρ is the threshold and δ is the average Voronoi area for a uniform distribution of localizations. After applying this first threshold, the intersection between the Voronoi polygon area distribution and the distribution of Voronoi polygon areas corresponding to the Monte Carlo simulation was identified and applied as the second threshold. This procedure was iterated multiple times to define several thresholds at increasing density.

Antibodies

The following antibodies were used in this study:

Antibodies	Company	cat#
Rabbit anti-H3K9me2	Active Motif	39239
Mouse anti-H3K9me2S10ph	Active Motif	61429
Rabbit anti-H3K9me3	Abcam	ab8898
Rabbit anti-H3K27me3	EMD Millipore	07-499
Rabbit anti-Lamin B1	Abcam	ab16048
Goat anti-Lamin B	Santa Cruz	sc-6216
Goat anti-Lamin B	Santa Cruz	sc-6217
Mouse anti-Lamin A/C	Santa Cruz	sc-376248
Mouse NPCs/mAb414	Abcam	Ab24609
Mouse anti-LMN1	HBUI	LMN1
Rabbit anti-histone H3	Abcam	ab1791
Rabbit anti-GFP	Abcam	ab290
Blocking peptides		
H3K9me2	Abcam	ab1772

H3K9me3	Abcam	ab1773
H3K27me2	Abcam	ab1781
H4K20me2	Abcam	ab14964
H3K9me0	EpiCypher	12-0001
H3K9me1	EpiCypher	12-0010
H3K9me2	EpiCypher	12-0011
H3K9me3	EpiCypher	12-0012
H3K9me2S10ph	EpiCypher	12-0093
Secondary Antibodies		
Donkey anti-rabbit AlexaFluor 555	Invitrogen	A11010
Donkey anti-Rabbit AlexaFluor 488	Invitrogen	A21206
Donkey anti-Rabbit AlexaFluor 568	Invitrogen	A10042
Donkey anti-Rabbit AlexaFluor 647	Invitrogen	A31573
Donkey anti-Mouse AlexaFluor 488	Invitrogen	A21202
Donkey anti-Mouse AlexaFluor 568	Invitrogen	A10037
Donkey anti-Goat AlexaFluor 488	Invitrogen	A11055
Donkey anti-Goat AlexaFluor 568	Invitrogen	A11057
Donkey anti-Goat AlexaFluor 647	Invitrogen	A21447
anti-rabbit IgG, HRP-linked	Cell Signaling	7074

539

540 **Antibody validation**

541 To test anti-H3K9me2 (Active Motif, cat#39239, lot#28214002) antibody specificity for
542 immunofluorescence assay, a set of short peptides mimicking histone tail lysine methylation was
543 used. H3K9me2 antibodies were preincubated with blocking peptides according to manufacturer's
544 recommendations (1µg of the antibody with 1µg of a peptide) in 1 ml of antibody blocking buffer
545 (1% BSA in PSBT), then used for immunostaining.

546

547 **DNA oligo FISH probe design and generation**

548 Target regions were based on constitutive LADs (LADs) or constitutive inter-LADs (non-LADs)
549 as previously defined (Meuleman et al., 2013). For LADs, regions were selected only if they were
550 also defined as LADs according to both LaminB and H3K9me2 ChIPseq data from (Poleshko et
551 al., 2017); for non-LADs, regions were selected only if they were also defined as non-LADs

552 according to both LaminB and H3K9me2 ChIPseq data from Poleshko et al., 2017 (Poleshko et
553 al., 2017). Two to three of each, LAD and non-LAD, regions per mouse autosome were chosen
554 for generation of DNA oligo libraries (Table S1). Oligopaint libraries were designed using the
555 OligoMiner pipeline (Beliveau et al., 2018). Sequences of 42 nucleotides of homology to the
556 regions of interest were mined from the mouse mm9 genome build using the default parameters of
557 OligoMiner. Each probe was designed to target a 250 kb region of sequence at a density of 4
558 probes/kb when possible. Single stranded probes were produced using PCR, T7 RNA synthesis,
559 and reverse transcription as described previously (Rosin et al., 2018).
560
561 **Western blot**
562 Lysates were run on 4-12% Bis-Tris protein gels (Invitrogen #NP0335) and blots were probed
563 with anti-GFP (Abcam #ab290, 1:5000) or anti-H3 (Abcam #ab1791, 1:7500) primary antibodies
564 according to the instructions of the manufacturer. Anti-rabbit HRP-conjugated secondary antibody
565 (Cell Signaling #7074) was used at 1:7500. Visualization was achieved using ECLPrime (GE Life
566 Sciences #RPN2232).
567
568 **ChIP-seq tracks**
569 The accession number for the ChIP-seq data referenced (Poleshko et al., 2017) is NCBI GEO:
570 GSE97878.
571
572 **Statistical analysis**
573 Statistical analyses were performed with Graphpad PRISM 8.0.1 software (Graphpad Software,
574 Inc.) using ANOVA one-way non-parametric Kruskal-Wallis test with multiple comparison
575 correction using Dunn's test, or unpaired non-parametric Student's t-test (Mann-Whitney).
576

577 **Supplemental Information**

578 Supplemental Information includes six supplemental figures, one supplemental table, and three
579 movies.

580

581

Supplemental Figure 1

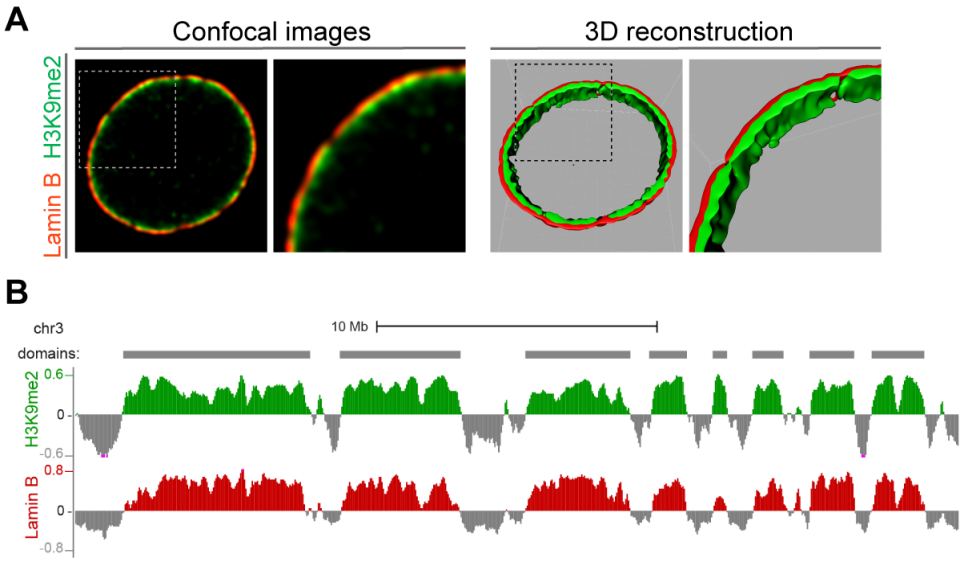

582

583

584

585 **Supplemental Figure S1. H3K9me2-marked chromatin localizes specifically at the nuclear periphery**
586 **and forms large heterochromatin domains. (A)** Representative confocal images of the H3K9me2-marked
587 chromatin (green) localizes at the nuclear lamina (Lamin B, red) of mouse ESCs. 3D-image reconstruction
588 (right panels) demonstrates H3K9me2 heterochromatin layer at the nuclear lamina. **(B)** Representative
589 H3K9me2 and Lamin B ChIP-seq tracks from mESCs illustrating lamina-associated domains specifically
590 enriched for H3K9me2 and Lamin B.

591

Supplemental Figure 2

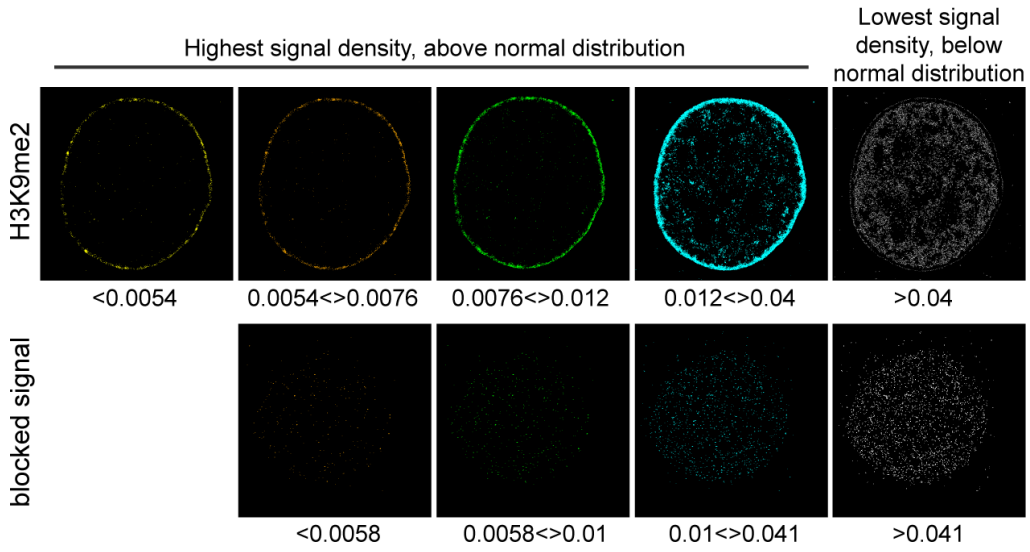

Supplemental Figure S2. H3K9me2 signal distribution is specific at the nuclear periphery. Representative STORM images of the H3K9me2 signal with or without blocking peptides after applying the automatic thresholding based on Voronoi tessellation (see methods) and shown from highest density (yellow) to lowest density (gray), illustrating separation of H3K9me2 and blocked signal. Specific H3K9me2 signal is localized at the nuclear periphery forming a layer of peripheral heterochromatin.

Supplemental Figure 3

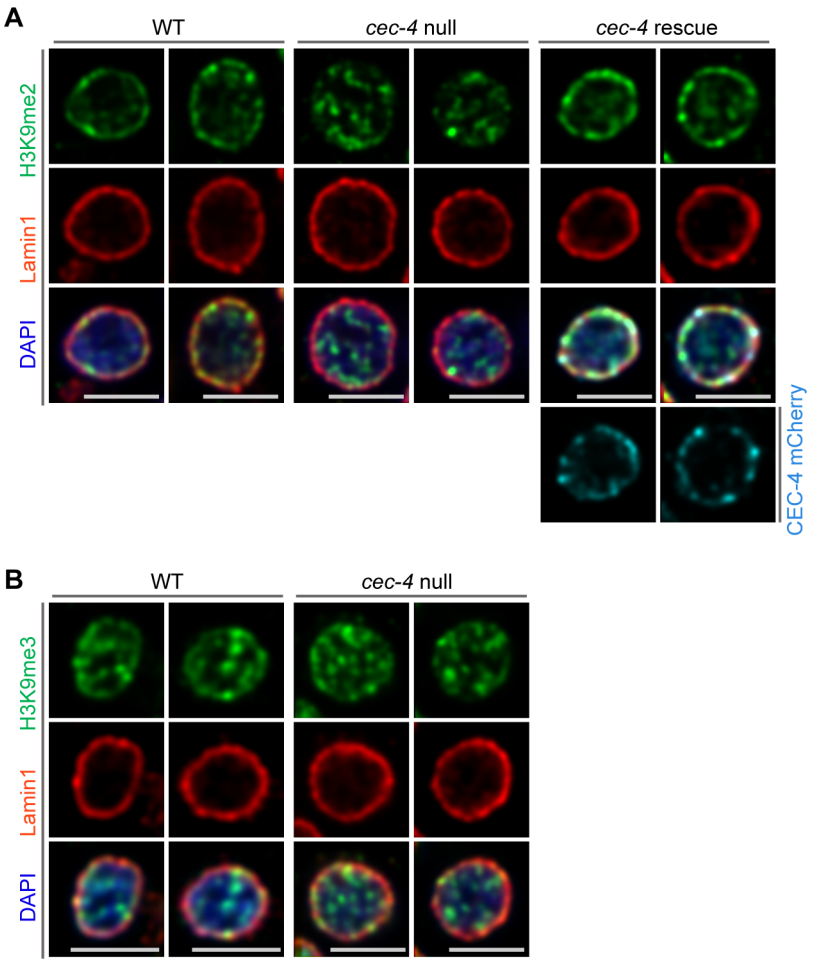

Supplemental Figure S3. Localization of H3K9me3-marked chromatin in *C. elegans* wild-type (WT), *cec-4*-null, and *cec-4*-rescue embryo cells. (A) Additional representative immunofluorescent confocal images of *C. elegans* embryo cells illustrate H3K9me2 (green) localized to the nuclear periphery as stained with Lamin1 (red) in WT and *cec-4*-null cells rescued with *cec-4* transgene (CEC-4 mCherry), but not in *cec-4*-null cells; counterstained with DAPI (blue). **(B)** Representative immunofluorescent confocal images illustrate H3K9me3 (green) distribution, counterstained with Lamin 1 (red) and DAPI (blue); Scale bars: 3μm.

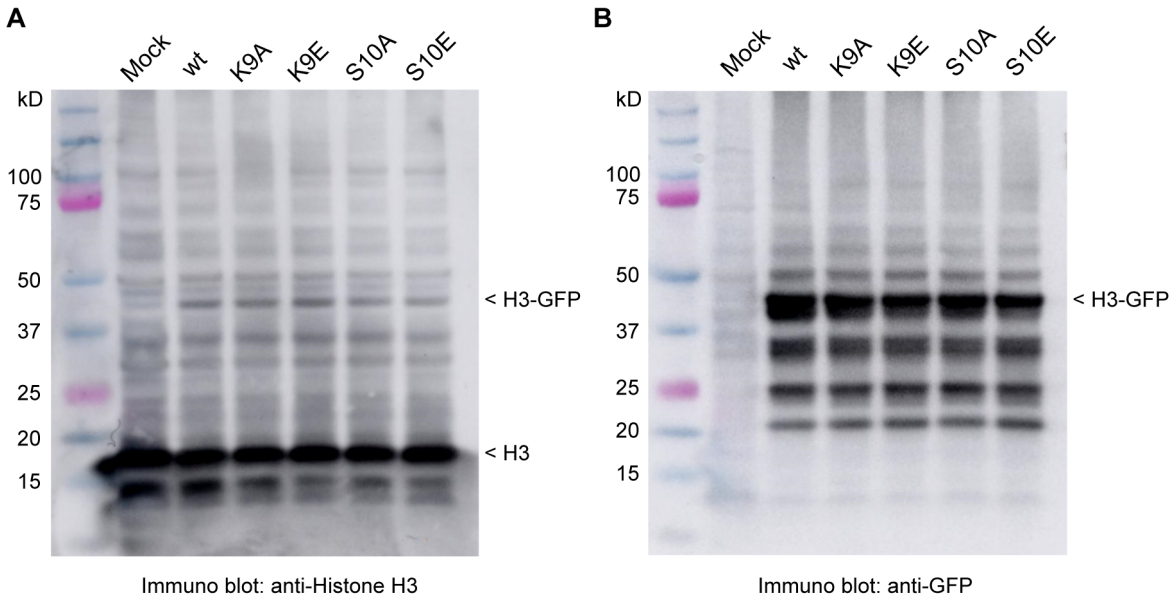

Immuno blot: anti-Histone H3

Immuno blot: anti-GFP

Supplemental Figure S4. Expression of histone H3-GFP fusion proteins. Histone H3 immunoblot demonstrating expression of exogenous H3-GFP fusion proteins. **(A)** anti-histone H3 immunoblot; and **(B)** anti-GFP immunoblot.

Supplemental Figure 5

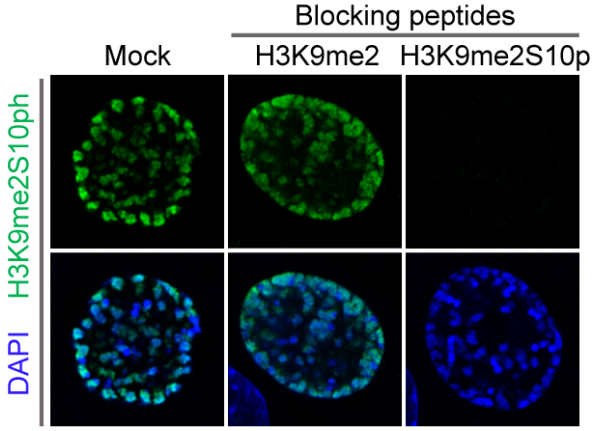

Supplemental Figure S5. Anti-H3K9me2S10p antibody specificity validation. C2C12 cells in prophase stained with H3K9me2S10p antibody preincubated with indicated blocking peptides, counterstained with DAPI.

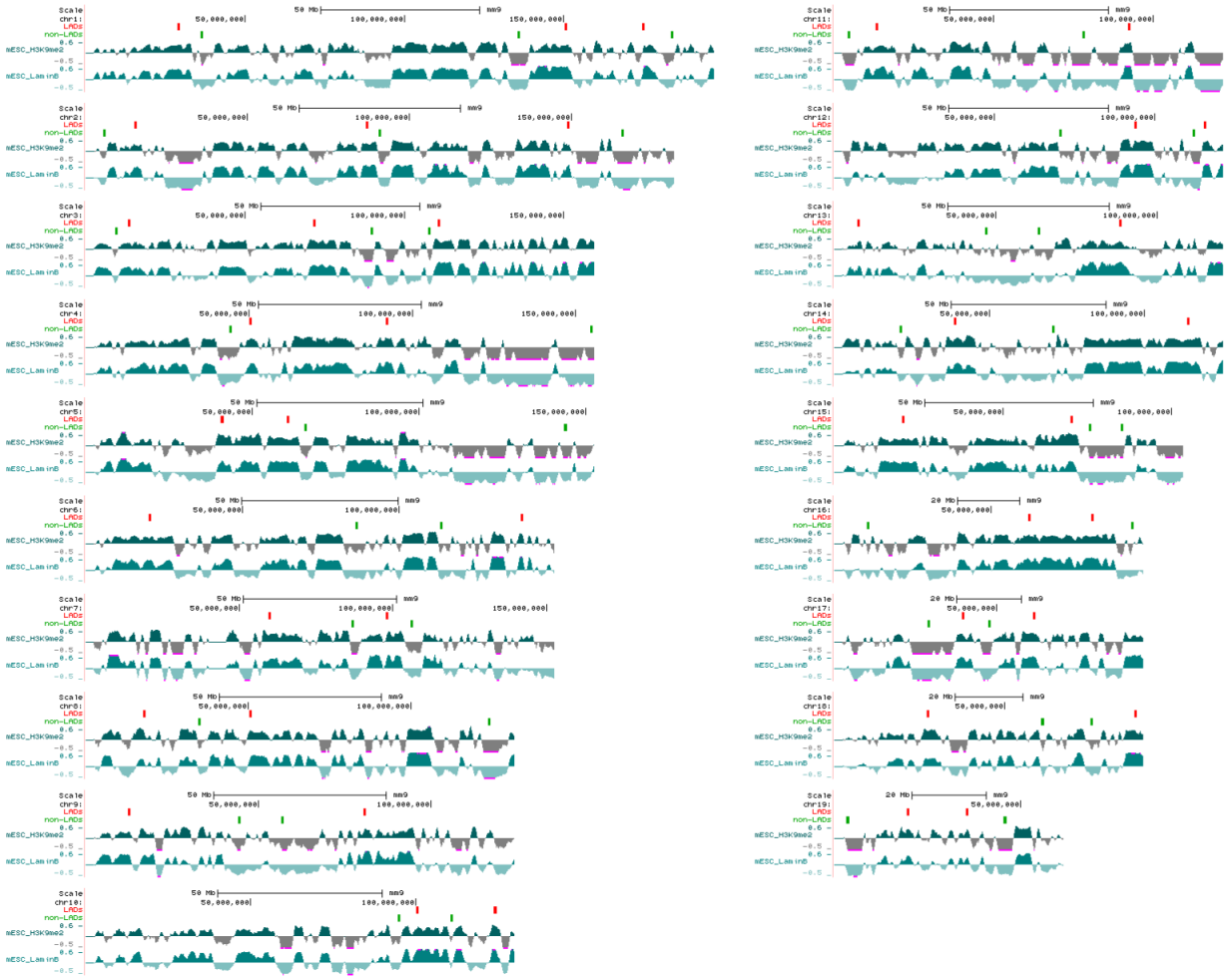

Supplemental Figure S6. Location of the oligopaint DNA probes targeting LADs and non-LADs on mouse chromosomes. Displayed are H3K9me2 and LaminB ChIP-seq tracks from mESCs with each region of 41 'LADs' (enriched for H3K9me2 and Lamin B signal) shown as a red bar above tracks and each region of 41 'non-LADs' (depleted for H3K9me2 and Lamin B) shown as a green bar; probes for each region span 250kb of the mouse genome (mm9).

631 **Supplemental Table S1.** Genomic coordinates (mm9) of regions targeted with oligopaint DNA probes.
632

	start	end	type	size			start	end	type	size
chr1	29104230	29354230	LAD	250000		chr1	36434433	36684433	non-LAD	250000
chr1	150673087	150923087	LAD	250000		chr1	135865407	136115407	non-LAD	250000
chr1	174920593	175170593	LAD	250000		chr1	183973123	184223123	non-LAD	250000
chr10	100527334	100777334	LAD	250000		chr10	94872520	95122520	non-LAD	250000
chr10	124051755	124301755	LAD	250000		chr10	110869061	111119061	non-LAD	250000
chr11	13179019	13429019	LAD	250000		chr11	4582747	4832747	non-LAD	250000
chr11	92370539	92620539	LAD	250000		chr11	77940228	78190228	non-LAD	250000
chr12	93813781	94063781	LAD	250000		chr12	70473766	70723766	non-LAD	250000
chr12	115634346	115884346	LAD	250000		chr12	111962534	112212534	non-LAD	250000
chr13	7489538	7739538	LAD	250000		chr13	47028288	47278288	non-LAD	250000
chr13	88441235	88691235	LAD	250000		chr13	63199709	63449709	non-LAD	250000
chr14	38703956	38953956	LAD	250000		chr14	21358915	21608915	non-LAD	250000
chr14	113906951	114156951	LAD	250000		chr14	70419884	70669884	non-LAD	250000
chr15	20289182	20539182	LAD	250000		chr15	75828606	76078606	non-LAD	250000
chr15	70422540	70672540	LAD	250000		chr15	85276609	85526609	non-LAD	250000
chr16	61890914	62140914	LAD	250000		chr16	10659379	10909379	non-LAD	250000
chr16	82120430	82370430	LAD	250000		chr16	94760705	95010705	non-LAD	250000
chr17	39538078	39783931	LAD	245853		chr17	28970900	29220900	non-LAD	250000
chr17	61496613	61746613	LAD	250000		chr17	47803613	48053613	non-LAD	250000
chr18	27523365	27738657	LAD	215292		chr18	61099822	61349822	non-LAD	250000
chr18	88450557	88700557	LAD	250000		chr18	75521659	75771659	non-LAD	250000
chr19	19633267	19883267	LAD	250000		chr19	3551051	3801051	non-LAD	250000
chr19	35509829	35759829	LAD	250000		chr19	45622537	45872537	non-LAD	250000
chr2	15379049	15629049	LAD	250000		chr2	5573731	5823731	non-LAD	250000
chr2	86720000	86970000	LAD	250000		chr2	90721129	90971129	non-LAD	250000
chr2	148980799	149230799	LAD	250000		chr2	165772679	166022679	non-LAD	250000
chr3	71596078	71846078	LAD	250000		chr3	9641987	9891987	non-LAD	250000
chr3	110735097	110985097	LAD	250000		chr3	89658552	89908552	non-LAD	250000
chr3	13525990	13775990	LAD	250000		chr3	107840306	108090306	non-LAD	250000
chr4	50271294	50521294	LAD	250000		chr4	44223436	44473436	non-LAD	250000
chr4	92067850	92317850	LAD	250000		chr4	154687066	154937066	non-LAD	250000
chr5	40813624	41063624	LAD	250000		chr5	65928768	66178768	non-LAD	250000
chr5	60638162	60884800	LAD	246638		chr5	143797763	144047763	non-LAD	250000
chr6	20389410	20639410	LAD	250000		chr6	86325063	86575063	non-LAD	250000
chr6	139025301	139275301	LAD	250000		chr6	113420393	113670393	non-LAD	250000
chr7	59721791	59971791	LAD	250000		chr7	86892565	87142565	non-LAD	250000
chr7	97983011	98233011	LAD	250000		chr7	105952531	106202531	non-LAD	250000
chr8	17936222	18186222	LAD	250000		chr8	34947799	35197799	non-LAD	250000
chr8	50541295	50791295	LAD	250000		chr8	123933822	124183822	non-LAD	250000
chr9	12396200	12646200	LAD	250000		chr9	44431734	44681734	non-LAD	250000
chr9	80651724	80901724	LAD	250000		chr9	56821780	57071780	non-LAD	250000

Movie S1. 3D reconstruction of mouse ES cells in interphase. Immunostained for Lamin B1 (cyan) and hybridized with fluorescent oligo probes for LADs (red) and non-LADs (green), and counterstained with DAPI (blue).

Movie S2. 3D reconstruction of mouse ES cells in metaphase. Immunostained for Lamin B1 (cyan) and hybridized with fluorescent oligo probes for LADs (red) and non-LADs (green), and counterstained with DAPI (blue).

Movie S3. 3D reconstruction of mouse ES cells in telophase. Immunostained for Lamin B1 (cyan) and hybridized with fluorescent oligo probes for LADs (red) and non-LADs (green), and counterstained with DAPI (blue).

References

AMENDOLA, M. & VAN STEENSEL, B. 2014. Mechanisms and dynamics of nuclear lamina-genome interactions. *Curr Opin Cell Biol,* 28**,** 61-8 DOI: 10.1016/j.ceb.2014.03.003.

ANDREY, G. & MUNDLOS, S. 2017. The three-dimensional genome: regulating gene expression during pluripotency and development. *Development,* 144**,** 3646-3658 DOI: 10.1242/dev.148304.

ANDRONOV, L., ORLOV, I., LUTZ, Y., VONESCH, J. L. & KLAHOLZ, B. P. 2016. ClusterViSu, a method for clustering of protein complexes by Voronoi tessellation in super-resolution microscopy. *Sci Rep,* 6**,** 24084 DOI: 10.1038/srep24084.

BELIVEAU, B. J., KISHI, J. Y., NIR, G., SASAKI, H. M., SAKA, S. K., NGUYEN, S. C., WU, C. T. & YIN, P. 2018. OligoMiner provides a rapid, flexible environment for the design of genome-scale oligonucleotide in situ hybridization probes. *Proc Natl Acad Sci U S A,* 115**,** E2183-E2192 DOI: 10.1073/pnas.1714530115.

BICKMORE, W. A. 2013. The spatial organization of the human genome. *Annu Rev Genomics Hum Genet,* 14**,** 67-84 DOI: 10.1146/annurev-genom-091212-153515.

BUCHWALTER, A., KANESHIRO, J. M. & HETZER, M. W. 2019. Coaching from the sidelines: the nuclear periphery in genome regulation. *Nat Rev Genet,* 20**,** 39-50 DOI: 10.1038/s41576-018-0063-5.

BURKE, B. & GERACE, L. 1986. A cell free system to study reassembly of the nuclear envelope at the end of mitosis. *Cell,* 44**,** 639-52 DOI.

COLLAS, P. 2010. The current state of chromatin immunoprecipitation. *Mol Biotechnol,* 45**,** 87-100 DOI: 10.1007/s12033-009-9239-8.

CREMER, C., SZCZUREK, A., SCHOCK, F., GOURRAM, A. & BIRK, U. 2017. Super-resolution microscopy approaches to nuclear nanostructure imaging. *Methods,* 123**,** 11-32 DOI: 10.1016/j.ymeth.2017.03.019.

DEKKER, J., BELMONT, A. S., GUTTMAN, M., LESHYK, V. O., LIS, J. T., LOMVARDAS, S., MIRNY, L. A., O'SHEA, C. C., PARK, P. J., REN, B., POLITZ, J. C. R., SHENDURE, J., ZHONG, S. & NETWORK, D. N. 2017. The 4D nucleome project. *Nature,* 549**,** 219-226 DOI: 10.1038/nature23884.

DEKKER, J., MARTI-RENOM, M. A. & MIRNY, L. A. 2013. Exploring the three-dimensional organization of genomes: interpreting chromatin interaction data. *Nat Rev Genet,* 14**,** 390-403 DOI: 10.1038/nrg3454.

DEKKER, J., RIPPE, K., DEKKER, M. & KLECKNER, N. 2002. Capturing chromosome conformation. *Science,* 295**,** 1306-11 DOI: 10.1126/science.1067799.

EBERLIN, A., GRAUFFEL, C., OULAD-ABDELGHANI, M., ROBERT, F., TORRES-PADILLA, M. E., LAMBROT, R., SPEHNER, D., PONCE-PEREZ, L., WURTZ, J. M., STOTE, R. H., KIMMINS, S., SCHULTZ, P., DEJAEGERE, A. & TORA, L. 2008. Histone H3 tails containing dimethylated lysine and adjacent phosphorylated serine modifications adopt a specific conformation during mitosis and meiosis. *Mol Cell Biol,* 28**,** 1739-54 DOI: 10.1128/MCB.01180-07.

FESTUCCIA, N., GONZALEZ, I., OWENS, N. & NAVARRO, P. 2017. Mitotic bookmarking in development and stem cells. *Development,* 144**,** 3633-3645 DOI: 10.1242/dev.146522.

FINLAN, L. E., SPROUL, D., THOMSON, I., BOYLE, S., KERR, E., PERRY, P., YLSTRA, B., CHUBB, J. R. & BICKMORE, W. A. 2008. Recruitment to the nuclear periphery can alter expression of genes in human cells. *PLoS Genet,* 4**,** e1000039 DOI: 10.1371/journal.pgen.1000039.

FISCHLE, W., TSENG, B. S., DORMANN, H. L., UEBERHEIDE, B. M., GARCIA, B. A., SHABANOWITZ, J., HUNT, D. F., FUNABIKI, H. & ALLIS, C. D. 2005. Regulation of HP1-chromatin binding by histone H3 methylation and phosphorylation. *Nature,* 438**,** 1116-22 DOI: 10.1038/nature04219.

FISCHLE, W., WANG, Y. & ALLIS, C. D. 2003. Binary switches and modification cassettes in histone biology and beyond. *Nature,* 425**,** 475-9 DOI: 10.1038/nature02017.

FLAVAHAN, W. A., DRIER, Y., LIAU, B. B., GILLESPIE, S. M., VENTEICHER, A. S., STEMMER-RACHAMIMOV, A. O., SUVA, M. L. & BERNSTEIN, B. E. 2016. Insulator dysfunction and oncogene activation in IDH mutant gliomas. *Nature,* 529**,** 110-4 DOI: 10.1038/nature16490.

FOISNER, R. & GERACE, L. 1993. Integral membrane proteins of the nuclear envelope interact with lamins and chromosomes, and binding is modulated by mitotic phosphorylation. *Cell,* 73**,** 1267-79 DOI.

GERACE, L. & BLOBEL, G. 1980. The nuclear envelope lamina is reversibly depolymerized during mitosis. *Cell,* 19**,** 277-87 DOI.

GILBERT, D. M. 2010. Cell fate transitions and the replication timing decision point. *J Cell Biol,* 191**,** 899-903 DOI: 10.1083/jcb.201007125.

GONZALEZ-SANDOVAL, A., TOWBIN, B. D., KALCK, V., CABIANCA, D. S., GAIDATZIS, D., HAUER, M. H., GENG, L., WANG, L., YANG, T., WANG, X., ZHAO, K. & GASSER, S. M. 2015. Perinuclear Anchoring of H3K9-Methylated Chromatin Stabilizes Induced Cell Fate in C. elegans Embryos. *Cell,* 163**,** 1333-47 DOI: 10.1016/j.cell.2015.10.066.

GUELEN, L., PAGIE, L., BRASSET, E., MEULEMAN, W., FAZA, M. B., TALHOUT, W., EUSSEN, B. H., DE KLEIN, A., WESSELS, L., DE LAAT, W. & VAN STEENSEL, B. 2008. Domain organization of human chromosomes revealed by mapping of nuclear lamina interactions. *Nature,* 453**,** 948-51 DOI: 10.1038/nature06947.

716 HALLEY-STOTT, R. P., JULLIEN, J., PASQUE, V. & GURDON, J. 2014. Mitosis gives a brief window
717 of opportunity for a change in gene transcription. *PLoS Biol,* 12**,** e1001914 DOI:
718 10.1371/journal.pbio.1001914.
719 HARAGUCHI, T., KOJIDANI, T., KOUJIN, T., SHIMI, T., OSAKADA, H., MORI, C., YAMAMOTO,
720 A. & HIRAOKA, Y. 2008. Live cell imaging and electron microscopy reveal dynamic processes
721 of BAF-directed nuclear envelope assembly. *J Cell Sci,* 121**,** 2540-54 DOI: 10.1242/jcs.033597.
722 HIROTA, T., LIPP, J. J., TOH, B. H. & PETERS, J. M. 2005. Histone H3 serine 10 phosphorylation by
723 Aurora B causes HP1 dissociation from heterochromatin. *Nature,* 438**,** 1176-80 DOI:
724 10.1038/nature04254.
725 HOLTZER, H., WEINTRAUB, H., MAYNE, R. & MOCHAN, B. 1972. The cell cycle, cell lineages, and
726 cell differentiation. *Curr Top Dev Biol,* 7**,** 229-56 DOI.
727 HSIUNG, C. C. & BLOBEL, G. A. 2016. A new bookmark of the mitotic genome in embryonic stem cells.
728 *Nat Cell Biol,* 18**,** 1124-1125 DOI: 10.1038/ncb3432.
729 KADAUKE, S. & BLOBEL, G. A. 2013. Mitotic bookmarking by transcription factors. *Epigenetics*
730 *Chromatin,* 6**,** 6 DOI: 10.1186/1756-8935-6-6.
731 KIND, J., PAGIE, L., DE VRIES, S. S., NAHIDIAZAR, L., DEY, S. S., BIENKO, M., ZHAN, Y.,
732 LAJOIE, B., DE GRAAF, C. A., AMENDOLA, M., FUDENBERG, G., IMAKAEV, M., MIRNY,
733 L. A., JALINK, K., DEKKER, J., VAN OUDENAARDEN, A. & VAN STEENSEL, B. 2015.
734 Genome-wide maps of nuclear lamina interactions in single human cells. *Cell,* 163**,** 134-47 DOI:
735 10.1016/j.cell.2015.08.040.
736 KIND, J., PAGIE, L., ORTABOZKOYUN, H., BOYLE, S., DE VRIES, S. S., JANSSEN, H.,
737 AMENDOLA, M., NOLEN, L. D., BICKMORE, W. A. & VAN STEENSEL, B. 2013. Single-cell
738 dynamics of genome-nuclear lamina interactions. *Cell,* 153**,** 178-92 DOI:
739 10.1016/j.cell.2013.02.028.
740 KOHWI, M., LUPTON, J. R., LAI, S. L., MILLER, M. R. & DOE, C. Q. 2013. Developmentally regulated
741 subnuclear genome reorganization restricts neural progenitor competence in Drosophila. *Cell,* 152**,**
742 97-108 DOI: 10.1016/j.cell.2012.11.049.
743 KUBBEN, N., VONCKEN, J. W. & MISTELI, T. 2010. Mapping of protein- and chromatin-interactions
744 at the nuclear lamina. *Nucleus,* 1**,** 460-71 DOI: 10.4161/nucl.1.6.13513.
745 KUMARAN, R. I. & SPECTOR, D. L. 2008. A genetic locus targeted to the nuclear periphery in living
746 cells maintains its transcriptional competence. *J Cell Biol,* 180**,** 51-65 DOI:
747 10.1083/jcb.200706060.

LEVET, F., HOSY, E., KECHKAR, A., BUTLER, C., BEGHIN, A., CHOQUET, D. & SIBARITA, J. B. 2015. SR-Tesseler: a method to segment and quantify localization-based super-resolution microscopy data. *Nat Methods,* 12**,** 1065-71 DOI: 10.1038/nmeth.3579.

MEULEMAN, W., PERIC-HUPKES, D., KIND, J., BEAUDRY, J. B., PAGIE, L., KELLIS, M., REINDERS, M., WESSELS, L. & VAN STEENSEL, B. 2013. Constitutive nuclear lamina-genome interactions are highly conserved and associated with A/T-rich sequence. *Genome Res,* 23**,** 270-80 DOI: 10.1101/gr.141028.112.

NAUMOVA, N., IMAKAEV, M., FUDENBERG, G., ZHAN, Y., LAJOIE, B. R., MIRNY, L. A. & DEKKER, J. 2013. Organization of the mitotic chromosome. *Science,* 342**,** 948-53 DOI: 10.1126/science.1236083.

NEWPORT, J. 1987. Nuclear reconstitution in vitro: stages of assembly around protein-free DNA. *Cell,* 48**,** 205-17 DOI.

OOMEN, M. E. & DEKKER, J. 2017. Epigenetic characteristics of the mitotic chromosome in 1D and 3D. *Crit Rev Biochem Mol Biol,* 52**,** 185-204 DOI: 10.1080/10409238.2017.1287160.

PALOZOLA, K. C., LERNER, J. & ZARET, K. S. 2019. A changing paradigm of transcriptional memory propagation through mitosis. *Nat Rev Mol Cell Biol,* 20**,** 55-64 DOI: 10.1038/s41580-018-0077-z.

PERIC-HUPKES, D., MEULEMAN, W., PAGIE, L., BRUGGEMAN, S. W., SOLOVEI, I., BRUGMAN, W., GRAF, S., FLICEK, P., KERKHOVEN, R. M., VAN LOHUIZEN, M., REINDERS, M., WESSELS, L. & VAN STEENSEL, B. 2010. Molecular maps of the reorganization of genome-nuclear lamina interactions during differentiation. *Mol Cell,* 38**,** 603-13 DOI: 10.1016/j.molcel.2010.03.016.

PHILLIPS-CREMINS, J. E., SAURIA, M. E., SANYAL, A., GERASIMOVA, T. I., LAJOIE, B. R., BELL, J. S., ONG, C. T., HOOKWAY, T. A., GUO, C., SUN, Y., BLAND, M. J., WAGSTAFF, W., DALTON, S., MCDEVITT, T. C., SEN, R., DEKKER, J., TAYLOR, J. & CORCES, V. G. 2013. Architectural protein subclasses shape 3D organization of genomes during lineage commitment. *Cell,* 153**,** 1281-95 DOI: 10.1016/j.cell.2013.04.053.

POLESHKO, A., MANSFIELD, K. M., BURLINGAME, C. C., ANDRAKE, M. D., SHAH, N. R. & KATZ, R. A. 2013. The human protein PRR14 tethers heterochromatin to the nuclear lamina during interphase and mitotic exit. *Cell Rep,* 5**,** 292-301 DOI: 10.1016/j.celrep.2013.09.024.

POLESHKO, A., SHAH, P. P., GUPTA, M., BABU, A., MORLEY, M. P., MANDERFIELD, L. J., IFKOVITS, J. L., CALDERON, D., AGHAJANIAN, H., SIERRA-PAGAN, J. E., SUN, Z., WANG, Q., LI, L., DUBOIS, N. C., MORRISEY, E. E., LAZAR, M. A., SMITH, C. L., EPSTEIN, J. A. & JAIN, R. 2017. Genome-Nuclear Lamina Interactions Regulate Cardiac Stem Cell Lineage Restriction. *Cell,* 171**,** 573-587 e14 DOI: 10.1016/j.cell.2017.09.018.

PRIGENT, C. & DIMITROV, S. 2003. Phosphorylation of serine 10 in histone H3, what for? *J Cell Sci,* 116**,** 3677-85 DOI: 10.1242/jcs.00735.

PROBST, A. V., DUNLEAVY, E. & ALMOUZNI, G. 2009. Epigenetic inheritance during the cell cycle. *Nat Rev Mol Cell Biol,* 10**,** 192-206 DOI: 10.1038/nrm2640.

PUESCHEL, R., CORAGGIO, F. & MEISTER, P. 2016. From single genes to entire genomes: the search for a function of nuclear organization. *Development,* 143**,** 910-23 DOI: 10.1242/dev.129007.

REDDY, K. L., ZULLO, J. M., BERTOLINO, E. & SINGH, H. 2008. Transcriptional repression mediated by repositioning of genes to the nuclear lamina. *Nature,* 452**,** 243-7 DOI: 10.1038/nature06727.

RICCI, M. A., COSMA, M. P. & LAKADAMYALI, M. 2017. Super resolution imaging of chromatin in pluripotency, differentiation, and reprogramming. *Curr Opin Genet Dev,* 46**,** 186-193 DOI: 10.1016/j.gde.2017.07.010.

ROBSON, M. I., DE LAS HERAS, J. I., CZAPIEWSKI, R., LE THANH, P., BOOTH, D. G., KELLY, D. A., WEBB, S., KERR, A. R. W. & SCHIRMER, E. C. 2016. Tissue-Specific Gene Repositioning by Muscle Nuclear Membrane Proteins Enhances Repression of Critical Developmental Genes during Myogenesis. *Mol Cell,* 62**,** 834-847 DOI: 10.1016/j.molcel.2016.04.035.

ROSIN, L. F., NGUYEN, S. C. & JOYCE, E. F. 2018. Condensin II drives large-scale folding and spatial partitioning of interphase chromosomes in Drosophila nuclei. *PLoS Genet,* 14**,** e1007393 DOI: 10.1371/journal.pgen.1007393.

SAWICKA, A. & SEISER, C. 2014. Sensing core histone phosphorylation - a matter of perfect timing. *Biochim Biophys Acta,* 1839**,** 711-8 DOI: 10.1016/j.bbagrm.2014.04.013.

STADHOUDERS, R., FILION, G. J. & GRAF, T. 2019. Transcription factors and 3D genome conformation in cell-fate decisions. *Nature,* 569**,** 345-354 DOI: 10.1038/s41586-019-1182-7.

STIERNAGLE, T. 2006. Maintenance of C. elegans. *WormBook***,** 1-11 DOI: 10.1895/wormbook.1.101.1.

SUREKA, R., WADHWA, R., THAKUR, S. S., PATHAK, R. U. & MISHRA, R. K. 2018. Comparison of Nuclear Matrix and Mitotic Chromosome Scaffold Proteins in Drosophila S2 Cells-Transmission of Hallmarks of Nuclear Organization Through Mitosis. *Mol Cell Proteomics,* 17**,** 1965-1978 DOI: 10.1074/mcp.RA118.000591.

TOWBIN, B. D., GONZALEZ-SANDOVAL, A. & GASSER, S. M. 2013. Mechanisms of heterochromatin subnuclear localization. *Trends Biochem Sci,* 38**,** 356-63 DOI: 10.1016/j.tibs.2013.04.004.

VARIER, R. A., OUTCHKOUROV, N. S., DE GRAAF, P., VAN SCHAIK, F. M., ENSING, H. J., WANG, F., HIGGINS, J. M., KOPS, G. J. & TIMMERS, H. T. 2010. A phospho/methyl switch at histone H3 regulates TFIID association with mitotic chromosomes. *EMBO J,* 29**,** 3967-78 DOI: 10.1038/emboj.2010.261.

WANDKE, C. & KUTAY, U. 2013. Enclosing chromatin: reassembly of the nucleus after open mitosis. *Cell,* 152**,** 1222-5 DOI: 10.1016/j.cell.2013.02.046.

WANG, F. & HIGGINS, J. M. 2013. Histone modifications and mitosis: countermarks, landmarks, and bookmarks. *Trends Cell Biol,* 23**,** 175-84 DOI: 10.1016/j.tcb.2012.11.005.

WEI, Y., YU, L., BOWEN, J., GOROVSKY, M. A. & ALLIS, C. D. 1999. Phosphorylation of histone H3 is required for proper chromosome condensation and segregation. *Cell,* 97**,** 99-109 DOI.

WINTER, S., SIMBOECK, E., FISCHLE, W., ZUPKOVITZ, G., DOHNAL, I., MECHTLER, K., AMMERER, G. & SEISER, C. 2008. 14-3-3 proteins recognize a histone code at histone H3 and are required for transcriptional activation. *EMBO J,* 27**,** 88-99 DOI: 10.1038/sj.emboj.7601954.

ZULLO, J. M., DEMARCO, I. A., PIQUE-REGI, R., GAFFNEY, D. J., EPSTEIN, C. B., SPOONER, C. J., LUPERCHIO, T. R., BERNSTEIN, B. E., PRITCHARD, J. K., REDDY, K. L. & SINGH, H. 2012. DNA sequence-dependent compartmentalization and silencing of chromatin at the nuclear lamina. *Cell,* 149**,** 1474-87 DOI: 10.1016/j.cell.2012.04.035.